A Proposal for the DarkLight Experiment at the Jefferson Laboratory Free Electron Laser

P. Balakrishnan, J. Bernauer, W. Bertozzi, R. Cowan, K. Dow, C. Epstein, P. Fisher *, S. Gilad, A. Kelleher, Y. Kahn, R. Milner, R. Russell, J. Thaler, C. Tschalaer, A. Winnebeck

Laboratory for Nuclear Science, Massachusetts Institute of Technology, Cambridge, MA 02139, USA

S. Benson, J. Boyce, D. Douglas, R. Ent, P. Evtushenko, H. C. Fenker, J. Gubeli, F. Hannon, J. Huang, K. Jordan, G. Neil, T. Powers, D. Sexton, M. Shinn, C. Tennant, S. Zhang

Jefferson Lab, 12000 Jefferson Avenue, Newport News, VA 23606

M. Freytsis

Physics Dept. U.C. Berkeley, Berkeley, CA

R. Fiorito, P. O'Shea

Institute for Research in Electronics and Applied Physics University of Maryland, College Park, MD

R. Alarcon, R. Dipert

Physics Department, Arizona State University, Tempe, AZ

G. Ovanesyan

Los Alamos National Laboratory, Los Alamos NM

M. Kohl

Physics Dept., Hampton University, Hampton, VA 23668 and Jefferson Lab, 12000 Jefferson Avenue, Newport News, VA 23606

T. Horn

Physics Dept., Catholic University of America, Washington, DC 20064

* Corresponding author (fisherp@mit.edu)

(Dated: December 1, 2010)

New theories of dark matter predict A' gauge bosons in the mass range of 0.01–10 GeV that couple to charged fermions with a strength of $\alpha'/\alpha_{\rm EM} = 10^{-4}$ of the photon or less. We propose to design, construct and operate an experiment called DarkLight (Detecting A Resonance Kinematically with eLectrons Incident on a Gaseous Hydrogen Target) to use the 1 MW 100 MeV electron beam at the Jefferson Lab Free Electron Laser incident on a 10^{19}cm^2 thick target to study the process $e^- + p \to e^- + p + e^- + e^+$. A dark force particle would show up as a narrow resonance in the radiated $e^+ - e^-$ system. Our experiment would explore the A' mass region 10-100 MeV and couplings as low as $\alpha' \sim 10^{-9}$ with 1/ab of data, which would require 60 days of data taking (assuming 100% efficiency) at the Jefferson Lab Free Electron Laser. We also plan for 30 days of running (assuming 100% efficiency) for beam studies, calibration and commissioning.

I. INTRODUCTION

Dark matter comprises 23% of the energy of the universe, and in the past ten years detection of dark matter and elucidation of its nature has moved to the forefront of experimental particle physics. Until recently, axions and weakly interacting massive particles (WIMPS) were the favored candidates and the focus of experimental investigation. Recent results, however, from both underground and cosmic ray experiments suggest that dark matter may be explained by a new theory that predicts vector or scalar bosons in the 10 MeV–10 GeV mass range that couple to electrons and positrons. Current experimental bounds limit the coupling to less than 10^{-2}–10^{-3} of the QED coupling, depending on the boson mass. This motivates us to consider experiments able to probe this new theory using a 1 MW, 100 MeV electron beam at the Jefferson Laboratory Free Electron Laser (FEL). In December 2009, we submitted a letter of intent to carry out a new experimental search using the JLab FEL. The LOI was favorably reviewed by PAC35. In the past year, we have formed the DarkLight collaboration which has developed a detailed technical concept for the experiment. This document describes the science case and technical concept for the DarkLight experiment with the aim of an unique and dedicated search for direct evidence for this new physics

beyond the Standard Model.

The DarkLight experiment is designed to search for a narrow resonance in the e+e- spectrum of elastic electron-proton scattering below pion threshold (i.e. at 100 MeV incident electron energy). Such a resonance will rest on the QED radiative tail. The final state proton recoils with low kinetic energy and DarkLight is designed to detect all final state particles using a large acceptance toroidal magnetic spectrometer. Vertex detectors for both recoil proton and final-state leptons are planned as well as large drift chambers in each sector of the magnetic toroid. The windowless gas target with multi-stage differential pumping system is embedded in the magnetic toroid.

II. PHYSICS MOTIVATION

Recent interest in new light bosons has been sparked by their possible connection to dark matter physics. Here, we summarize the dark matter motivation for new A' bosons, and list some existing experimental constraints and search strategies.

A. Dark Matter and Dark Forces

By now, the gravitational evidence for dark matter is overwhelming [1–4]. While the precise nature and origin of dark matter is unknown, thermal freezeout of a weakly interacting massive particle (WIMP) is a successful paradigm that arises in many theories beyond the standard model. In the WIMP paradigm, dark matter is a TeV-scale particle that interacts with standard model particles via electroweak interactions. There is a wide range of searches that are sensitive to WIMPs, including direct detection in nuclear recoil experiments, direct production in collider experiments, and indirect detection in cosmic ray experiments.

In the past two years, however, a new paradigm for dark matter has emerged where dark matter is still a TeV-scale particle, but interacts dominantly through a "dark force" [5–8]. The carrier for this (short-range) force is a new GeV-scale particle, which we refer to as A'. To confirm this new paradigm, one would like to gain direct evidence for this A' boson.

These dark force models are motivated by three astrophysical anomalies that hint at excess electron/positron production in the Milky Way: the WMAP Haze [9, 10], the PAMELA, FERMI, and H.E.S.S. e^+/e^- excesses [11–14], and the INTEGRAL 511 keV excess [15, 16].

Such dark force models may also play a role in explaining the DAMA annual modulation signal [17]. Intriguingly, these anomalies can be explained in terms of dark matter annihilation, decay, and/or up-scattering in the Milky Way halo, though not with a standard WIMP. Rather, the peculiar features of these anomalies hint that dark matter is interacting with a light A' boson and that A' bosons are being produced in these dark matter interactions. To explain the anomalies while evading other astrophysical bounds, the A' boson must dominantly decay to electrons, muons, pions and/or taus, with little hadronic activity [18–20]. In addition, the most recent e^+e^- data gives a Standard Model prediction for $(g-2)_\mu$ which lies 3.6 σ away from the measurement [21]. Corrections from a dark force carrier in the 10–100 MeV range could explain this difference.

There are a variety of different dark force scenarios, but the most popular models invoke a new vector boson that kinetically mixes with the standard model photon [6, 7]:

$$\mathcal{L} = \epsilon F'_{\mu\nu} F^{\mu\nu}_{\rm EM}. \tag{1}$$

Through this "photonic portal", the A' boson inherits electromagnetic couplings, albeit with a reduced coupling strength

$$\alpha' = \epsilon^2 \alpha_{\rm EM}, \tag{2}$$

where $\alpha_{\rm EM} \sim 1/137$. The coupling α' and the mass $m_{A'}$ are both free parameters in these models. While other dark force models are equally plausible, we focus on the photonic portal case for concreteness, since it is the one most studied in the literature.

B. Searching for the Dark Force

Spurred by this new dark force paradigm, there has been much recent interest on how to find the light A' boson. There is a huge range of $\{\alpha', m_{A'}\}$ values that are consistent with existing astrophysical measurements, so multiple experiments will be necessary to probe the full parameter space. To date, a number of possible avenues for discovery have been explored, including:

- Production in lepton colliers through $e^+e^- \to \gamma + X$ [22–28]. When A' decays promptly to $\mu^+\mu^-$, existing B-factory data already places a constraint.

- Production in fixed-target experiments. Previous searches for light axions are also sensitive to A' bosons if A' is sufficiently long-lived [29, 30]. There are ongoing effort

to do data mining on prior experiments, and Refs. [26, 31, 32] include a number of new fixed-target proposals. Of particular relevance for Jefferson Lab, the APEX experiment has completed a trial run in Hall A, and the HPS experiment is proposed for Hall B.

- Rare meson decays [23, 26, 33, 34]. Any meson decay that yields a photon could have a suppressed branching fraction to a dark photon. In particular, a reanalysis of KTeV data [35] would be sensitive to $\pi^0 \to \gamma + X$ with $X \to e^+e^-$.

- Production in fixed-target experiments with a positron beam [36].

However, the muon anomalous magnetic moment results pick out the region $m_{A'}$ =10-100 MeV [23, 34], so DarkLight focusses on this region.

The goal of the present proposal is to study couplings in the range $10^{-9} < \alpha' < 10^{-6}$, and masses in the range 10 MeV $< m_{A'} <$ 100 MeV. In this parameter range, the A' boson dominantly decays promptly as $A' \to e^+e^-$ with $c\tau > 10^{-2}$ cm. This parameter space is illustrated in Fig. 1, with the most important constraints indicated. We believe we can reach couplings in the range $\alpha' = 10^{-9} - 10^{-7}$ over the mass range 10–90 MeV with a 60 days (assuming 100% efficiency) of running at the JLab FEL.

1. Other physics topics

A search for invisible modes in $e^- + p \to e^- + p$: In addition to the recent interest in $A' \to e^+e^-$[61], there is additional motivation for light A' bosons that dominantly decay invisibly. The INTEGRAL 511 keV excess [15] could be interpreted as coming from sub-10 MeV dark matter in the galactic center annihilating through an off-shell A' to e^+e^- pairs [37–40]. This A' has both a coupling to e^+e^- pairs as well as to light dark matter particles χ, and in the preferred region of parameter space, the dominant decay is $A' \to \chi\chi$. One can therefore search for an invisibly decaying A' boson by looking for the process $ep \to ep + A'$ with $A' \to$ inv.

There was in fact a proposal to search for such an invisibly decaying A' boson using an energy recovery linac in Ref. [41], but that proposal did not have full kinematic reconstruction, and was unable to control radiative QED backgrounds. With the DarkLight experiment, we will have the ability to fully reconstruct the $ep \to ep +$ inv. process, and partially veto

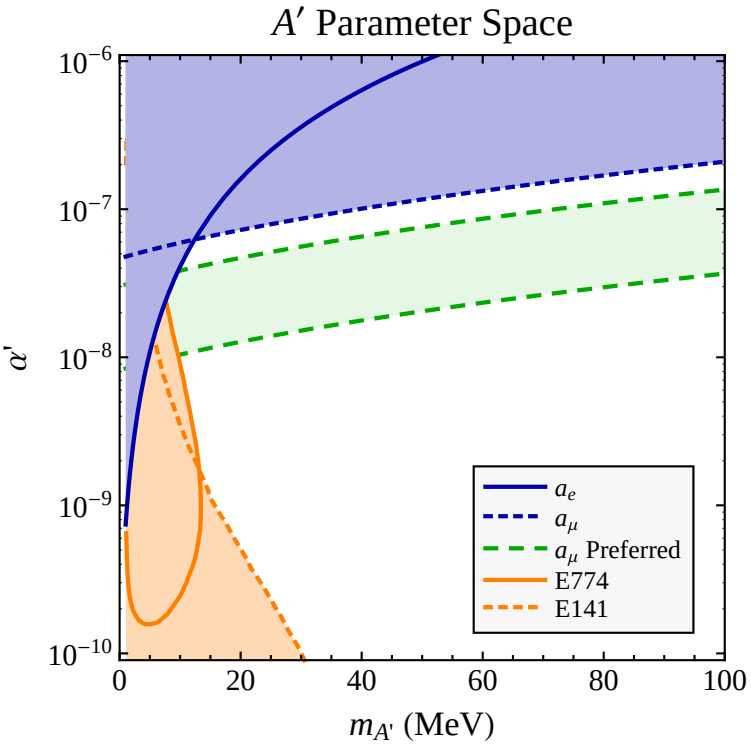

FIG. 1: The A' boson parameter space considered in the proposed search. The blue shaded regions correspond to bounds on the anomalous magnetic moment of the electron (a_e) and muon (a_μ) [23, 34]. The A' boson can actually reconcile the 3.6σ discrepancy with the measured value of a_μ in the "a_μ Preferred" region.. The orange shaded regions correspond to bound from previous beam dump experiments, E774 at Fermilab [30] and E141 at SLAC [29], where the A' boson is sufficiently long-lived to yield a displaced vertex.

photons from the processes $ep \to ep+\gamma$ and $ep \to ep+\gamma\gamma$ which can fake an invisible signal. We are working on developing the experimental concept and so do not yet have a clear idea of the sensitivity.

Measurement of the proton charge radius using $e-p$ scattering: The electromagnetic form factors of the proton at low Q^2 have long been one of the interesting measurements in the standard model. Such measurements have gained renewed interest with the recent measurement of the muonic Lamb shift [42], which suggest a different value of proton charge radius than previous extractions using ep scattering data [43–45] and determinations from spectroscopy of electronic hydrogen [46–48]. Since the proton charge radius

$\langle r_p^2 \rangle$ is defined in terms of the slope of the electric form factor $G_p^E(Q^2)$ as

$$\langle r_p^2 \rangle = -6 \left. \frac{\mathrm{d}G_p^E(Q^2)}{\mathrm{d}Q^2} \right|_{Q^2=0}$$

precise and accurate measurements of $G_p^E(Q^2)$ can be used to extract the proton charge radius and compare to the recent measurements.

With an electron beam energy of 100 MeV and an electron acceptance between 25° and 165°, DarkLight is sensitive to Q^2 values in ep elastic scattering between 0.0019 $(\mathrm{GeV}/c)^2$, a factor of 2 smaller value than [45], and 0.033 $(\mathrm{GeV}/c)^2$, with even lower values accessible with a lower beam energy and extended forward acceptance.

Using a model for G_p^M, the proton charge radius can be extracted from a measurement at one energy alone, since the cross section at forward angles and low Q^2 is dominated by the electric form factor.

A variation of the beam energy will allow us to separate the form factors using the Rosenbluth technique model independently. The comparatively small Q^2 values even at backward angles give us the opportunity to determine both G_p^E and G_p^M with good precision in this low Q^2 regime, where only few reliable data points exist. Such a separation would also yield precise charge and magnetization radii. While it is hard to determine the absolute cross section with uncertainties small enough to add a meaningful data set to the world data, it should be possible to fix the global normalization with an extrapolation of the cross section or of the form factors to $Q^2 = 0$, where their values are known, a method already used in [45]. In the upcoming month, we plan to work out the feasibility of this method.

Weak interaction studies in $e - p$ scattering: The charged current electroweak reaction

$$\vec{e} + p \rightarrow \vec{\nu}_e + \vec{\Lambda}$$

may be studied using DarkLight. For a typical MeV scale cross sections, an integrated luminosity of 1/ab should yield a few events. The hyperon's decay into a charged pion and proton may then be used to determine the hyperon polarization in this reaction. An interesting kinematic cusp effect at production threshold (electron energy 197 MeV) gives a sizeable enhancement in the cross section. An experimental measurement of the weak axial-vector form factor in this reaction may then be feasible with the DarkLight setup if there is running at electron energies above pion threshold.

III. THE FREE ELECTRON LASER

As the only currently operating free electron laser (FEL) based on a CW superconducting energy recovering linac (ERL), the Jefferson Laboratory FEL Upgrade remains unique as an FEL driver [49, 50]. The present system represents the culmination of years of effort in the areas of SRF technology, ERL operation, lattice design, high power optics and DC photocathode gun technology. The layout of the JLab FEL Facility is shown in Fig. 2. The machine as it stands delivers 7 micron emittance bunches of 135 pC at average currents up to 10 mA (74.85 MHz repetition rate). The present beam energy is 135 MeV although it has operated up to 160 MeV in the past. The system has lased in the 0.364 to 11 micron region and produced up to 14.3 kW of average power at 1.6 microns. At lower powers it can tune rapidly over factors of 8 in wavelength. The stable performance of this machine over many years establishes a solid foundation for future light sources and other applications such as the experiment proposed in this report.

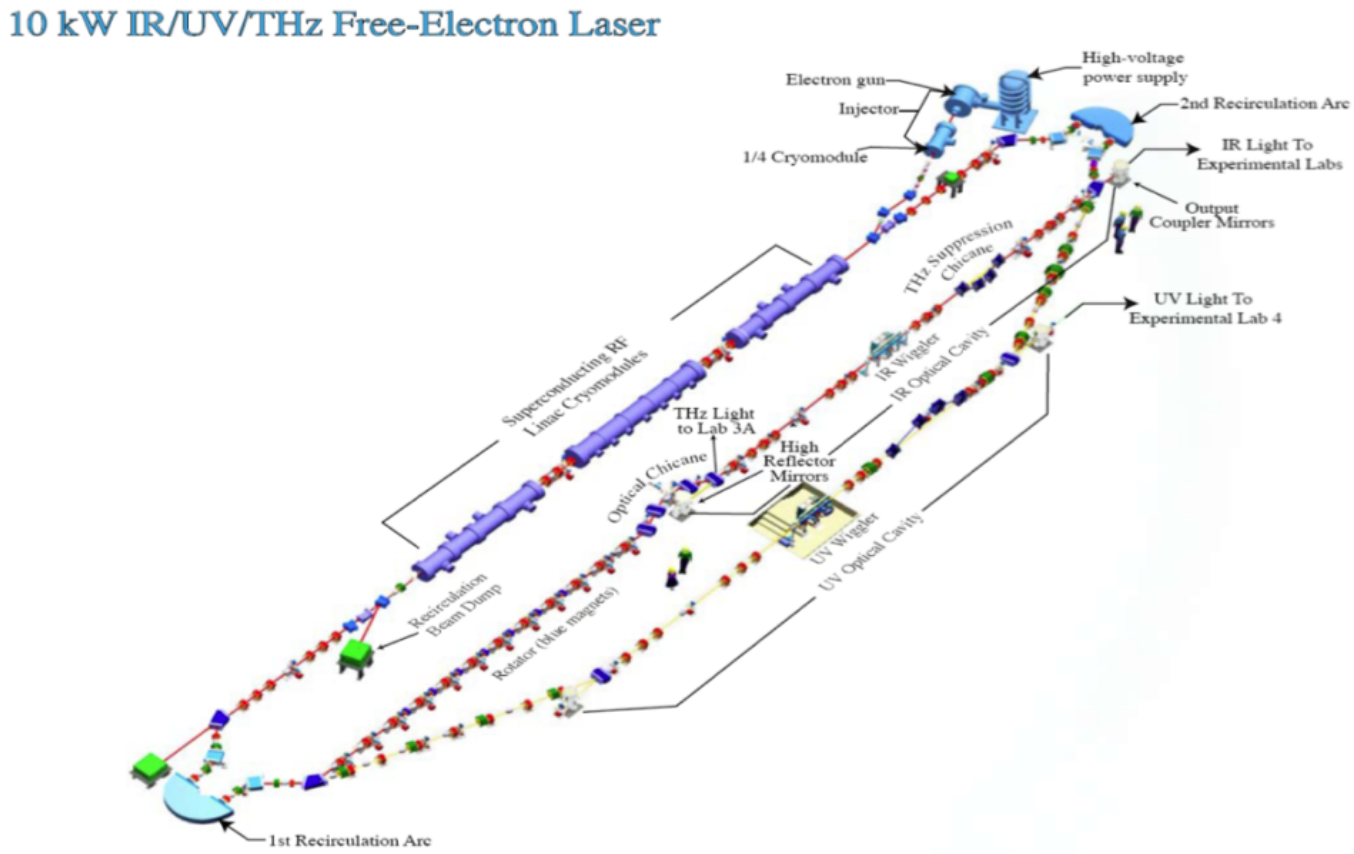

FIG. 2: Schematic of the existing JLab light source facility.

The ERL accelerator is comprised of a 9 MeV injector generating up to 9.3 mA of current (nominally in bunches of up to 135 pC at a maximum rep. rate of 74.85 MHz), a linac consisting of three Jefferson Lab cryomodules generating a total of 80 to 125 MeV of energy gain, and a recirculator. The latter provides beam transport to, and phase space conditioning of, the accelerated electron beam for the FELs and then returns and prepares the drive beam for energy recovery in the linac. The beam is typically accelerated (energy recovered) off crest (off trough) so as to impose a phase energy correlation on the longitudinal phase space used in subsequent transport to longitudinally match the beam to the required phase space at the wiggler (dump). That is to say, the bunch is kept relatively long during acceleration, compressed to high peak current and approximately 100 fs rms pulse lengths just before the wiggler, then temporally expanded before reinsertion into the energy recovery phase of the linac. The recirculation transport is, however, operationally flexible and can accommodate configurations providing very small momentum spread to users - though at commensurately longer bunch length.

The electron beam can be sent through the IR wiggler beam path or through the UV wiggler. Switching between the operational modes is accomplished by shorting half the coils of the corner dipoles. The energy recovery transport consists of a second Bates-style end loop followed by a six-quad telescope. The beam is matched to the arc by the second telescope of the FEL insertion; the energy recovery telescope matches beam envelopes from the arc to the linac acceptance. During FEL operation, energy recovery occurs off-trough. The imposed phase-energy correlations are selected to generate energy compression during energy recovery, yielding a long, low momentum spread bunch at the dump. Calculations and measurements show that the emittance growth due to Coherent Synchrotron Radiation (CSR) is not a problem for lower charges but may impact operation at higher charge. As indicated above, this operating mode can be modified to provide small momentum spread and longer bunches; this will alleviate CSR-driven beam quality degradation.

For the proposed DarkLight experiment, the machine will operate in either a different on-crest acceleration scheme or with a cross-phased tuning, so as to provide smaller momentum spread and longer bunch, instead of the nominal off-crest now used for FEL operation. It is desired that both beam-halo and emittance be eventually measured at the experimental location - the UV wiggler pit. In view, however, of up-coming FEL programmatic activities (including removal of the current UV wiggler and installation of a new one, and an IR FEL

run for the Navy program), schedule constraints in the near term motivate performing initial halo measurements in the 3F region on the IR line. This choice has the added advantage of performing initial halo studies in the most operationally flexible and heavily instrumented region of the system.

The FEL has gained extensive experience and has in place the necessary beam controls to deal with halo along the beam line. However, it will be necessary to remove the halo-monitor from its legacy position downstream of the second recirculation arc and reinstall it in a cross near 3F06 region on the IR line. In regard to the relevance of halo measurements at the IR beamline as opposed to on the UV beamline, it has been pointed out that although this location is not where the DarkLight experiment is eventually intended to take place, the measurement will provide valuable experience and data needed for a preliminary beam analysis, uncover potential effects that may be seen in the final location, and thus inform the design of the beam line to the DarkLight detector in the UV section of the ERL accelerator.

It is desirable for this experiment to run the accelerator at lower energy (100 MeV), low charge (10-20pC), and high repetition rate (748.5MHz) in order to reduce the emittance of the electron beam. In order to run the machine this way for the DarkLight experiment, certain modifications and additions to the electron photocathode gun drive laser and to the injector tuning are needed, which will be detailed in the following discussion.

A. Roadmap to DarkLight ERL Operation

Present performance of the JLab FEL ERL Driver is largely consistent with DarkLight requirements, save for demonstration of the specific machine setup and adequate halo characterization and management. We propose a three-step route to prepare the ERL for DarkLight production runs.

The initial step will be a test intended to provide an existence proof of a machine configuration which will allow adequate halo management. In order to complete this activity in a timely manner and at low cost, this test will be performed on the IR side of the system. A halo monitor (currently installed after the second recirculation arc, see section III B) will be modified (as required to allow it to mimic DarkLight aperture constraints), and moved to the FODO array upstream of the final bunch compressor near 3F06 region. This region of the machine is heavily instrumented, provides a large number of focusing and steering

controls, and has an installed nonlinear element (an octopole) that has already been used to modify large amplitude components of the beam during beam tuning.

We have at least two options for the test. The first involves a modification of the 5-quad rotator, removing the center skew quad and retuning the remaining four quads to provide the required Horizontal-Vertical (H-V) phase space interchange (there is a proof-of-principle solution for this tuning that will be tested before any beamline modifications occur). This option is attractive in that it will allow operation of the machine at full current during the halo test. The second alternative is to replace one of the existing beam line viewers in the FODO array with the halo monitor. This will allow testing with tune-up beam and/or at CW currents up to the order of 1 mA, but this option may generate beam envelopes outside of the acceptance of the H-V interchange and may as a consequence preclude operation above the "nominal" beam break up (BBU) threshold. In either case, we will explore halo as a function of single bunch charge, and thus test the option of running very high rep rate at low charge (748.5 MHz x 13.5 pC) as a space-charge-induced halo mitigation method.

The second step will be to characterize halo so as to provide the information required to manage it at the location of the DarkLight detector. This will be done using two studies, one presently under way and one proposed. The first study, performed by a collaboration lead by the UMD [51], uses a masking method to capture and characterize halo behavior (see subsection III C). The second study involves large dynamic range (LDR) measurements of beam properties (see subsection III D).

With measurement of emittance at high current and the degree of mismatch of the halo relative to the core beam, we will be positioned to complete an analysis of the beam properties and finalize the beamline design required to inject the beam into the DarkLight detector in the UV ERL wiggler pit. In this final step, we will (given a choice of bunch charge and injection parameters) complete the longitudinal matching scenario, perform an analysis of beam quality preservation (e.g. with space charge), develop a finalized optics design (including, as needed, H-V interchange and nonlinear envelope management using octopoles), and certify error sensitivities using start-to-end simulation. The finalized solution will be tested on the UV ERL, and halo studies repeated so as to check/optimize procedures for background mitigation once the detector is installed. This activity will include a thorough exploration of the acceptance of the UV recovery transport so as to define the maximum scattering amplitude (and thus the target density and interaction rate) that can be recovered

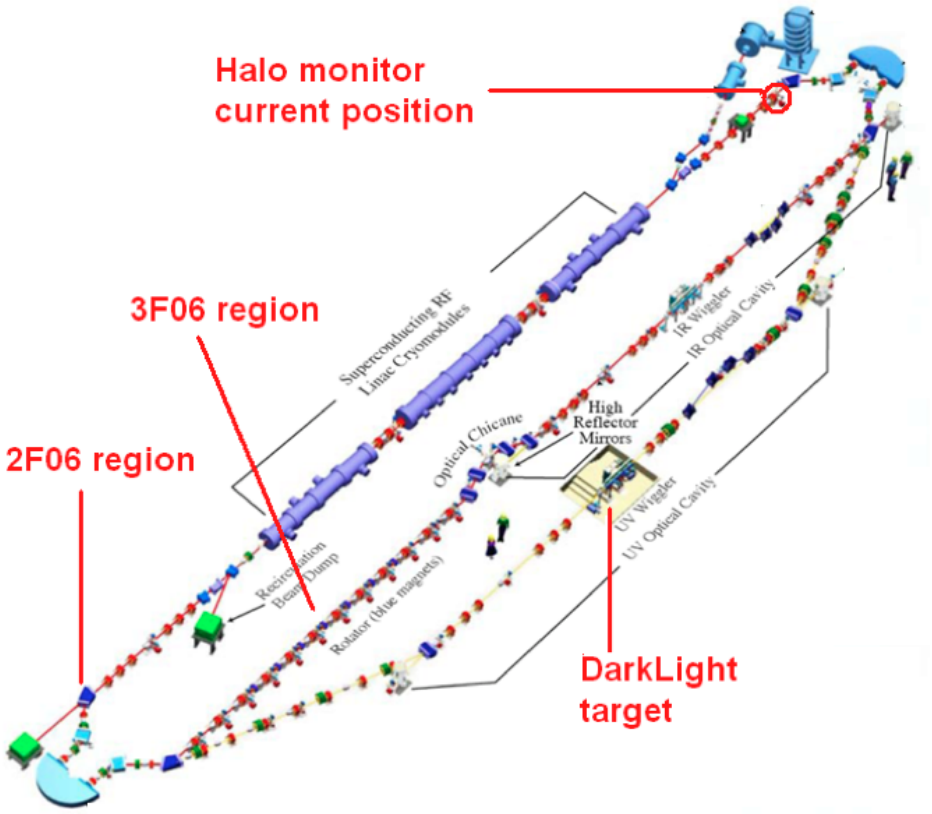

FIG. 3: Illustration of key positions along the JLab ERL accelerator beamline.

without intolerable beam loss.

The following sections provide detail about specific work activities and hardware needed to implement the aforementioned tests and measurements.

B. Measurement of Beam-halo with an Existing Halo Monitor

As mentioned earlier, a time and cost effective approach to measure the beam halo would be to remove the existing interceptive halo monitor including the 6-way cross currently installed at the beginning of the linac reinjection region and re-locate it in the middle of the infrared backleg region (near 3F06, see Fig. 3). There is a skew quad currently in that location. The minimum aperture from the current halo monitor is limited to about 5mm, and some reconfiguration (such as off-setting the translation axis and reworking the phosphor forks) will be needed to reduced the aperture size to more closely simulate the

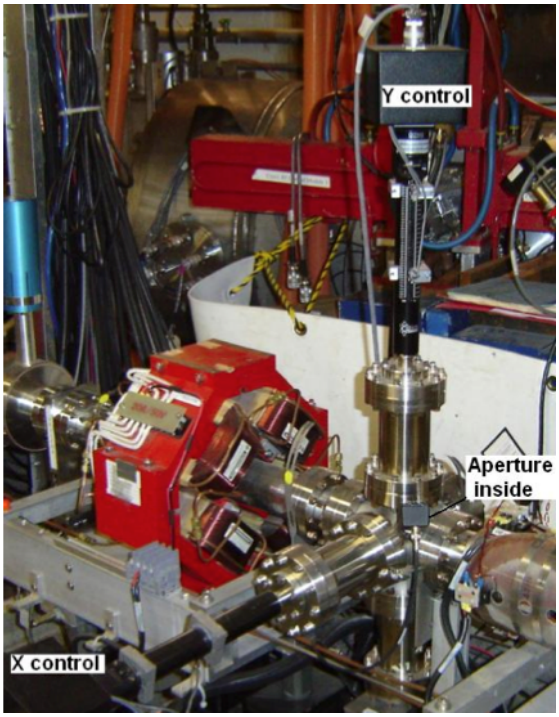

FIG. 4: Existing halo-monitor at 5F10 region.

smaller (2mm in diameter) aperture of the DarkLight experiment.

Fig. 4 is a picture of the currently existing interceptive beam halo monitoring device located at 5F05 near injector in the FEL vault. The device consists of two 6 stepper motor driven actuators, each fitted with a stepped fork (shown in Fig. 5). A variable step aperture is formed when the two forks move and cross to each other. There is an additional UV LED to illuminate to forks so the camera can be calibrated. When the device is moved the ion pump would remain connected to a replacement Tee, thus minimizing configuration change.

The forks are made of 1/16 Aluminum plate machined in steps of 10mm x 5mm (each side). When inserted all the way they close off the beam path completely. The position is calibrated against the external indicator (steps per mm) and the device is fitted with IN/OUT limit switches. The camera that monitors the device is in-line connected to the tangent point of the last dipole in the second arc. Radiation monitors (BLM PMTs, see more discussion in subsection III F) can also be used to monitor the intercepted beam.

The new location for the interceptive beam Halo monitor would be downstream of the quad girder 3F06. This would require the skew quad be temporarily removed and that an alternative phase-space exchange [52] be implemented. The Halo monitor would be fitted

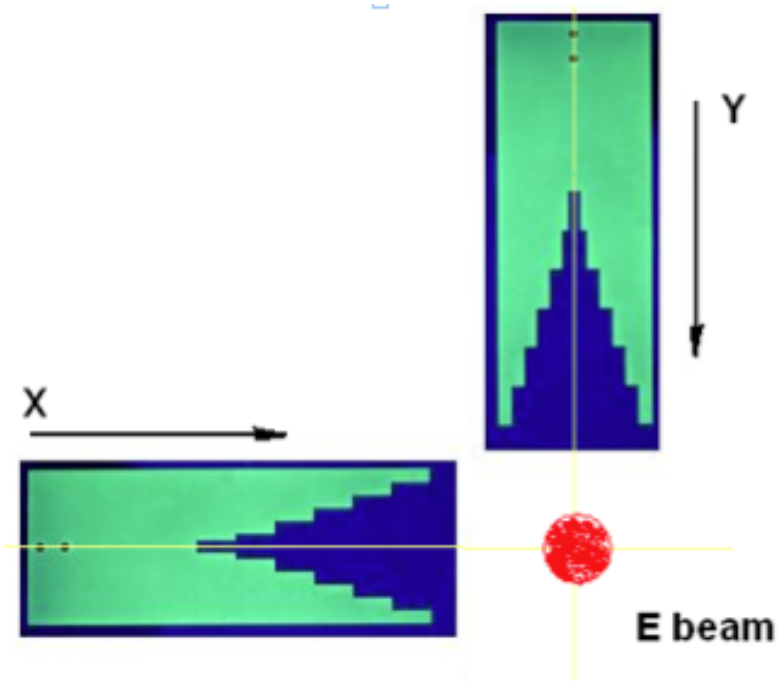

FIG. 5: Halo forks with steps of 5mm x 10mm. Proper off-set on X and Y axis will allow to measure smaller beam size.

to the existing stand now vacated. The camera view port would again be the tangent point at the last dipole of (now) the first arc. This is used as a HeNe alignment launch point in the current configuration.

C. Non-invasive Beam-halo Measurement

The goal of this activity is to establish a dedicated non-invasive halo monitor for the Dark-Light experiment without any disruption to the beam operation. This will be accomplished using Optical Synchrotron Radiation (OSR) which is parasitically produced at chicanes in both the IR and UV lines. We plan to design a flexible optical transport system that can allow observations of the OSR from either the IR or UV lines. Vault ceiling penetrations for either line and are relatively close to ports where the SR can be observed.

The current ceiling penetration for the UV wiggler cables will become available once the UV wiggler is removed, thus providing possibility for the SR light to be transported out of the FEL vault for non-invasive beam-halo measurement. There are a few places where a viewport exists or can be installed to view the SR light. For example, the viewport (clear

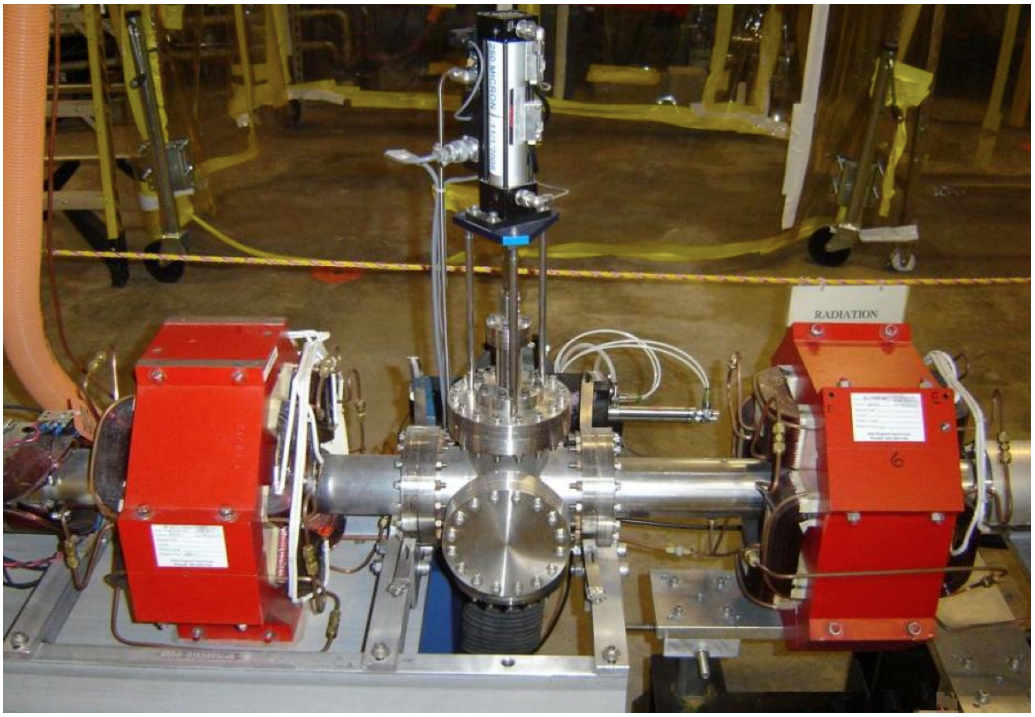

FIG. 6: Picture of quads at 3F06 region on IR beamline. The skew quad is the one on the right.

aperture 35mm in diameter) on the first bending magnet in the chicane up stream of the IR wiggler is immediately available. For the upcoming test in FEL in May, this will be an ideal spot to measure the beam-halo distributions. The electron beam can be imaged through this port the same way as the SR diagnostic system currently setup at 2F06 region. However, a different design of the optical transport is needed in order to do this. A sketch of the relative positions of the viewport and the SR beam path in the FEL vault are shown in Fig. 7. This estimate is subject to revision as details are refined.

A similar optical transport system will have to be built when the DarkLight detector is installed in the UV wiggler pit. Basically this only requires a modification of the optical system in the FEL vault. The optical components parts on the 2nd floor used for the IR line can be readily adopted to save costs.

D. Large Dynamic Range Beam Emittance Measurement

The beam emittance both upstream and downstream of the UV FEL wiggler location can be measured by quad scans using currently installed viewers. Such measurements were performed recently and the data is being analyzed. It should be pointed out that there are

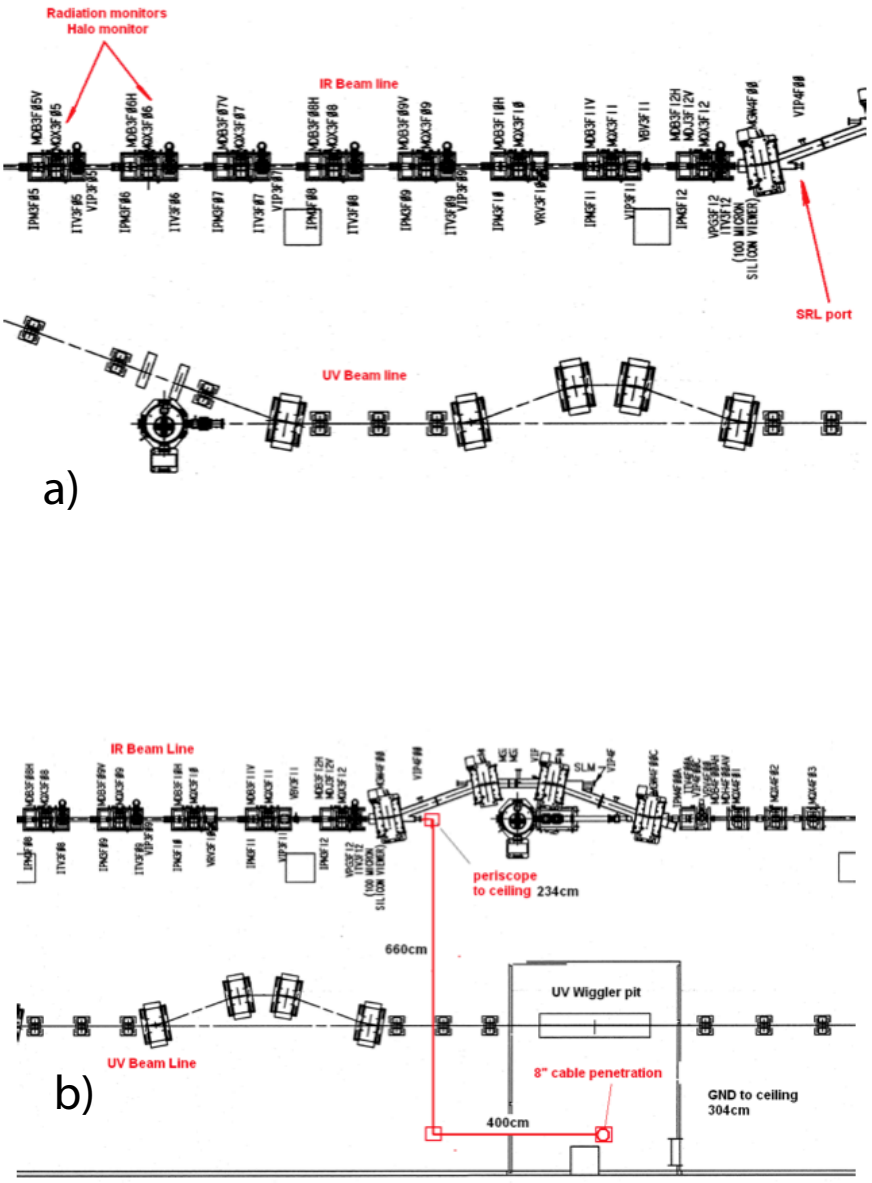

FIG. 7: a) Illustration of intended measurement sites. b) Schematic of beam path for SR optical transport in FEL vault.

more specific details associated with the beam profile and halo issue for such measurement, which are briefly addressed below.

To study the beam distribution in transverse phase space with large (10^5-10^6) dynamic range (LDR), the traverse beam profile needs to be measured over a similar dynamic range and with tune-up beam. In contrast to measurements using CW beam, the electron beam optics can be changed significantly when operating the tune-up beam. This will allow for

emittance measurements of the core of the beam as well as the halo of the beam - the part of the distribution with small intensity and potentially large betatron amplitude. When making measurements with tune-up beam, the integrated charge available for the measurement is significantly smaller. Thus, such imaging measurements must employ the process that is most efficient in converting electron beam into light. For LDR measurements with the tune-up beam we will therefore use 100 μm thin optically polished YAG:Ce crystal scintillators. Such beam viewers are already used at the JLab FEL for beam measurements in the injector. Operational experience indicates that with tune-up beam the intensity of the fluorescence will be sufficient for the measurements with the dynamic range of at least 10^5 or even 10^6. Such measurements will be based on use of two cameras, each with dynamic range of about 10^3 and attenuation effectively different by 10^3 to cover the required range.

E. Upgrade of machine operation mode

Although we will start DarkLight preparation with the currently available 74.85MHz repetition rate and perform important characterizations using bunch charges including 13.5 pC, as mentioned in section III B, it is deemed necessary to reconfigure the machine for operation at higher (748.5 MHz) repetition rate.

Unlike FELs which put stringent requirement on both transverse and longitudinal emittance, the DarkLight experiment only requires high average beam current and small transverse emittance; it places fewer constraints on the longitudinal phase space. This introduces the possibility of running the accelerator at a much lower bunch charge and at a higher pulse repetition rate. A recent study by F. Hannons shows a much lower emittance may be achieved from the FEL injector with a low bunch charge (approximately 20pC), as shown in Fig. 8. This presents a significant improvement of the e-beam quality and brightness over the present beam which is about 7-8 μm for 135pC bunch charge. It is very straightforward for the accelerator to run a beam at any sub-harmonic frequency of its 1.497GHz driving RF frequency. The question is if we can reconfigure the FEL drive laser to run at a high repetition rate that meets the requirement.

The FEL photo-cathode drive laser is a new laser system built on the state-of-the-art solid-state laser technology. Ever since it was commissioned, substantial reconfiguration and improvements have been made to keep up with the changing needs for machine operation

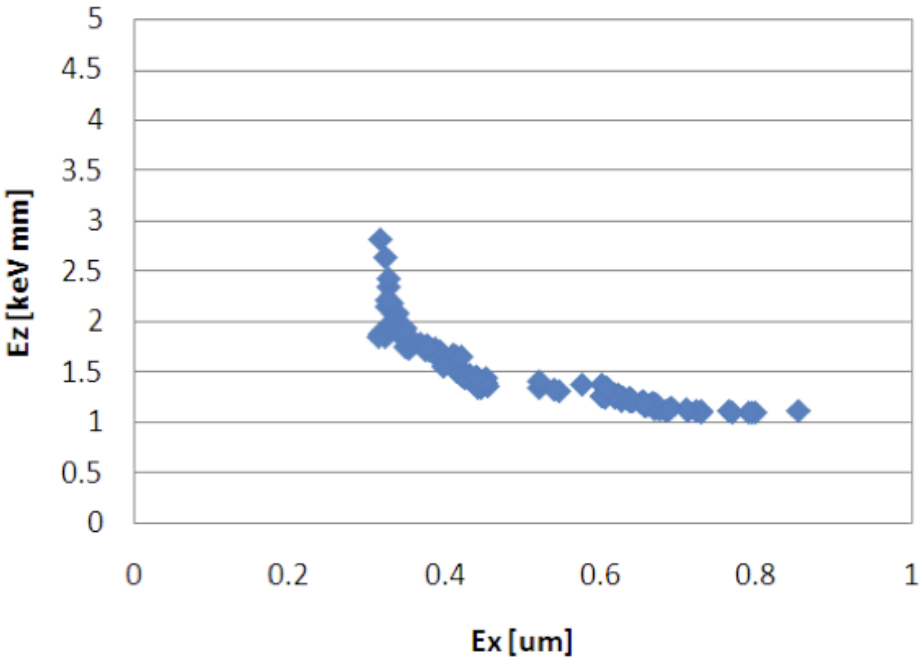

FIG. 8: Result of a beam emittance simulation for 20pC bunch charge from JLab FEL injector.

and various R&D projects. This diode-pumped all-solid-state laser system consists of several sections [53], the oscillator which produces seed pulses, the multi-stage amplifiers, second-harmonic generator (SHG), the beam relay, and pulse control system.

The seed laser is a custom-built diode-pumped Nd:YVO4, passively mode-locked oscillator with 25 ps pulse width and over 500 mW output power at 1064 nm. This oscillator can be operated at two distinctively different repetition rates, one is 74.85 MHz (the 20th sub-harmonic of 1.497 GHz) and the other 748.5 MHz (2nd sub-harmonic of 1.497 GHz). The optical configuration has to be changed in order to switch to a different pulse repetition rate. The synchronization to the accelerator is achieved by phase-locking the laser to the RF drive signal. A phase loop actively adjusts the optical cavity length to minimize the pulse timing jitter. The rms timing jitter is usually about 0.5 ps. The amplification system contains four identical diode-pumped amplification modules. The first two amplifiers form a lower power channel (Channel 1) with over 20 W output. When all four amplifiers are running, the maximum power can reach 50 W (output Channel 2). After amplification, the fundamental 1064 nm beam is frequency-doubled to 532 nm in a nonlinear crystal harmonic generator. At 74.85 MHz, the full laser power at 532 nm reaches 8 W from channel 1 and

25 W from channel 2. At 748.5MHz, about 13W was achieved due to lower SHG efficiency.

With the existing FEL photocathode, about 4 W of average laser power at 532nm is needed to generate 10 mA electron beam current. Therefore the available laser power is sufficient if we run drive laser at 748.5 MHz and 10-20 pC bunch charge (the average beam current will be about 10 mA). However, some upgrades over the existing system have to be done before the accelerator machine can operate under such a new beam mode. Specifically, we will need,

1. A new phase control system for 748.5 MHz laser oscillator. The key electronic components inside the phase-loop control chassis have to be replaced to accommodate the higher fundamental frequency. In addition, a new commercial phase-locking unit has to be purchased.

2. Upgrade of the drive laser pulse control system (DLPC) that currently only works at a maximum frequency of 74.85 MHz. The DLPC allows the accelerator to run at various beam-modes, in particular the tune-up mode at low duty-cycle routinely required by the machine optimization.

3. New electro-optic elements and drivers with much faster response.

4. Faster photo-detectors for pulse temporal pulse monitoring.

5. New laser pump diodes to replace the old ones in the laser.

F. Radiation monitors and measurement

To monitor the radiation level or beam loss near the diagnostics and the target, it is necessary to install a modest number of new beam loss probes in the FEL vault. We have had discussions and meetings with the JLab Radiation Control (RadCon) Group in order to make full use of their expertise and understand available resources.

There are basically several options for the detectors to use. The first option is that we can utilize RadCons infrastructure that exists within the FEL and install additional probes and base units. We already have a rapid access monitoring system which is functioning much the way expected for this proposed measurement.

The other option would be to check other vendors for probes that would satisfy the requirements for the measurements. The infrastructure for these units would need to be developed in order to read out these detectors. This is where the information from the suggested calculation and simulations will determine the detector requirements.

It is recommended that proper calculations and/or simulations be performed to help predict the potential radiation based on the present and expected FEL beam parameters such as energy, beam current and potential interaction targets. Also it would be useful to have multiple detectors of both neutron and gamma type at different distances, which may allow measurement of the radiation spectrum. This would be very helpful to the ultimate DarkLight experiment.

IV. EXPERIMENTAL DESIGN

In this section, the conceptual design of the DarkLight detector and target are described. The goal is to measure elastic electron proton scattering below pion threshold using the 100 MeV electron beam of the JLab FEL. With 10 mA of electron beam incident on a windowless gas target of thickness 10^{19} hydrogen atoms/cm^2, a data taking luminosity of 6×10^{35} cm^{-2} s^{-1} is attained. In 60 days of 100% efficient data taking, an integrated luminosity of 1 ab^{-1} is acquired at two different magnetic field settings. The experiment is designed to detect in coincidence with high efficiency the scattered electron, the recoil proton and the produced positron-electron pair. The identification of all the final state particles allows the determination of the full event kinematics and efficient background rejection. The design of the DarkLight experiment is guided by the experience of members of the collaboration with the BLAST experiment at MIT-Bates [54] and the OLYMPUS experiment now in preparation at DESY [55].

A. Design Considerations

1. Elastic scattering rate

Elastic scattering presents the major process and background source. The cross-section for elastic electron-proton scattering can be written as

θ deg.	E' MeV	T_p MeV	Q^2 $(\mathrm{MeV/c})^2$	$\sin^2\theta/2$	θ_q deg.	rate MHz
15	99.6	0.4	677	0.017	82.5	148
30	98.6	1.4	2642	0.067	77	17
45	97.0	3.0	5665	0.146	66	5
90	90.4	9.6	18080	0.5	42	0.3
135	84.6	15.4	28899	0.854	21	0.2
155	83.1	16.9	31677	0.953	11	0.06

TABLE I: Kinematics and rates for elastic electron-proton scattering in the DarkLight experiment. E' is the scattered electron energy, θ is the angle with respect to the electron beam direction and θ_q is the angle the recoil proton momentum vector makes with the beam axis.

$$\frac{d\sigma}{d\Omega} = \frac{4\alpha^2 E'^2 \cos^2\frac{\theta}{2}}{\sin^4\frac{\theta}{2}} \cdot \left[\frac{G_E^2 + \tau G_M^2}{1+\tau} + 2\tau G_M^2 \tan^2\frac{\theta}{2}\right] \tag{3}$$

where $\tau = \frac{Q^2}{4M^2}$ with M the proton mass; $G_E(Q^2) = [1 + Q^2/0.71\mathrm{GeV}^2]^{-2} \approx 1$; $G_M(Q^2) = 1.79 \cdot [1 + Q^2/0.71\mathrm{GeV}^2]^{-2} \approx 1.79$.

The elastic electron-proton cross-subsection has been calculated as a function of θ and the rate into bins of $\pm 2.5^\circ$ in θ and covering 2 π in azimuthal angle, i.e. $\Delta\Omega = 2\pi \sin\theta \Delta\theta$ determined. A luminosity of 6×10^{35} cm^{-2} s^{-1} has been assumed. The angle that the recoil proton makes with the incident electron beam θ_q is also calculated for each value of θ. The rates are summarized in Table I

2. QED background rate

The QED background process $e^- p \to e^- p e^+ e^-$ represents a smooth, irreducible background process for DarkLight on which the peak representing the decay of the A$'$ is sought. It has been calculated in detail in [56] which has been used extensively in the design described in this proposal. For example, the QED trigger rate within the acceptance of the detector described here is estimated at about 1 kHz, which is a manageable rate.

3. Summary of design constraints

The DarkLight detector must be able to detect with high efficiency an electron-positron-proton final state in the presence of a large QED background rate. This leads to a number of design constraints as follows:

- A magnetic field is required to both provide an invariant mass resolution of order 1 MeV and to shield the detectors from background process, e.g. Moller scattering and showering from halo particles. The field integral is estimated at 0.25 Tesla-meter and this is provided by a six coil toroidal spectrometer. The toroid will accept all scattered electrons from 25° to 165 °.

- Leptons from 5 MeV to 100 MeV must be tracked within the toroid. Six large drift chambers, one in each sector, will be used to track the leptons. These are similar in design to those used in the BLAST experiment at MIT-Bates. In addition, a scintillator hodoscope will be configured in each sector to provide a primary trigger for the leptons.

- The target will be a windowless storage cell with three stages of differential pumping on each side of the target. The target window must be be thin ($\approx$ 30 microns of kapton) to allow 1 MeV protons to exit.

- The final state proton will have a kinetic energy from about 1 to about 5 MeV. A gas TPC with very thin entrance window will be located around the gas target to detect the low energy, recoiling protons. This will be in the trigger.

- The elastic rate peaks in the forward direction for the final-state electron and at around 90° for the final state proton. By building a detector with no electron acceptance forward of 25° one would reduce the elastic rates very significantly. The minimum angle of detection needs to be determined in the context of maximizing the signal-to-noise. Correspondingly, the recoil proton rates are peaked at angles $\approx 90°$. The recoil protons from events where an e^+e^- pair is produced are all located forward of about 60° - see top right panel of Fig. 14 from [56].

- The total elastic electron-proton rate for a detector with electron detection only for $\theta > 30°$ and for proton detection $\theta_q < 60°$ is of order a few MHz from the above table.

B. Magnet

To meet the physics goals we have chosen a non-focusing spectrometer with a 6-coil toroidal configuration. Toroidal configurations offer several attractive practical features: a return yoke is not needed, compensating magnets are not necessary for operation of the electron beam, and essentially a field-free region is provided along the beam-target interaction profile. Tracking detector systems can be designed that occupy the space between the coils which allow for ample solid angle coverage.

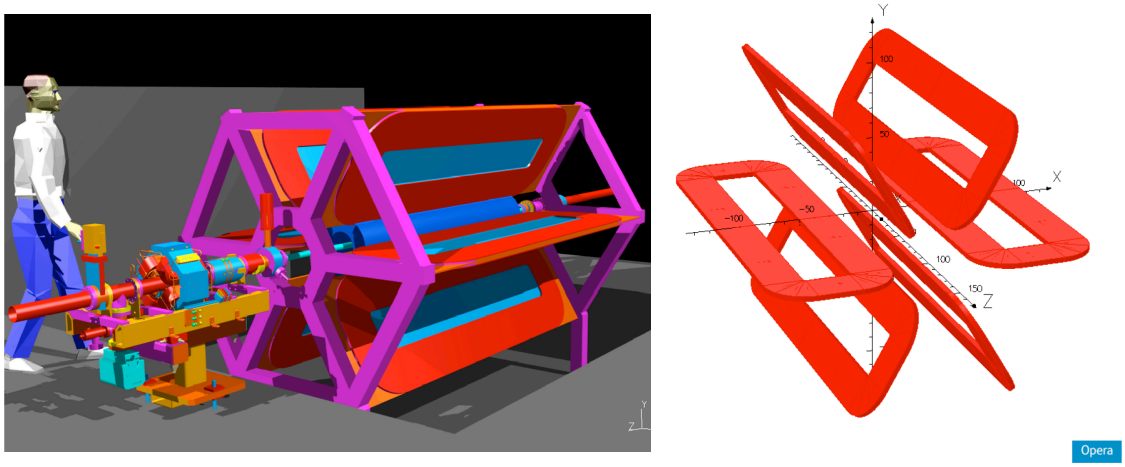

FIG. 9: Engineering concept of the toroid in the FEL available beamline (left) and the 6-coil configuration as modeled using the OPERA software (right).

As a starting point we have modeled a system that fits into existing available space at the FEL. Fig. 9 shows an engineering concept of the toroid in the current FEL beamline (left) and the 6-coil configuration modeled with the OPERA software (right). The center of the coils arrangement coincides with the center of the long internal gas target. The coils are 2 m long along the beam direction with an inner radius of 25 cm and outer radius of 105 cm.

Magnetic filed profiles have been calculated assuming coil cross sections of 3 by 25 cm^2 for four current densities: 2300, 1500, 1000, and 750 A/cm^2. These values correspond to total currents of 1.035, 0.675, 0.450, and 0.338 MA-turns, respectively. Fig. 10 (top) shows the magnitude of the magnetic field (essentially azimuthal) as a function of the radial distance along lines originating at 90^0 from the center of the interaction point. The integral of the

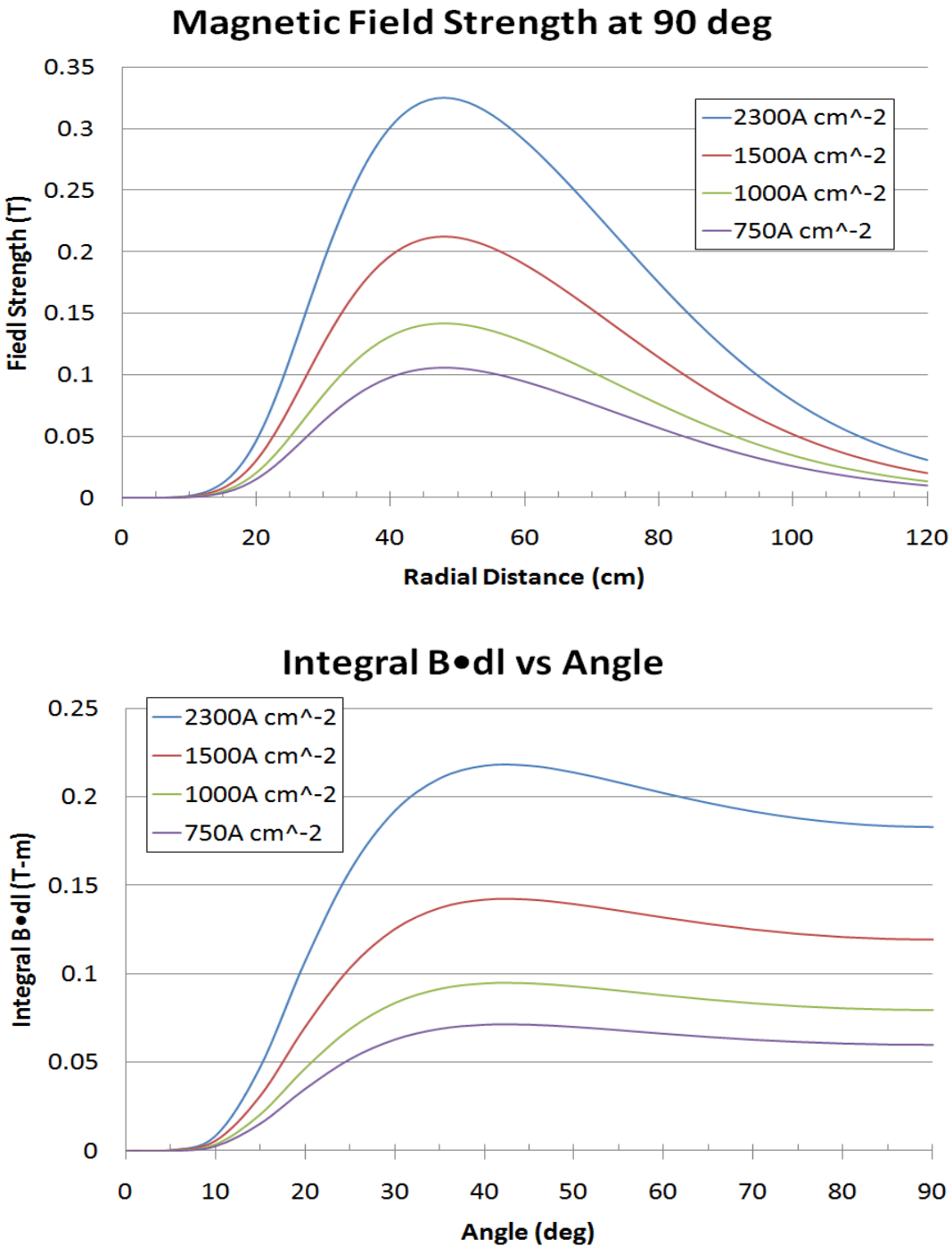

FIG. 10: Top: the magnitude of the magnetic field as a function of the radial distance along lines originating at 90^2 from the center of the interaction point. Bottom: The integral of the magnetic field in (Tesla-m) as a a function of the scattering angle for trajectories at different scattering angles.

magnetic field in (Tesla-m) is shown also in Fig. 10 (bottom) as a a function of the scattering angle for trajectories at different scattering angles. For the 1.035 MA-turns the values of the field integral match well with those demanded by the required electron resolution. The other configurations provide less field integral but allow better detection of low-energy electrons. These models seem to cover well the parameter space of the magnet design and a good starting point for a final technical design.

We have calculated the trajectories of elastic scattering electrons from hydrogen for the above magnetic field configurations. The scattered electron angles and energies correspond to those used in Table I. The trajectories are shown in Fig. 11 where at a given angle and energy those that bend slightly more correspond to the 1.035 MA-turn configuration. The trajectories are drawn in the $y - z$ plane, where y is the vertical direction and z the beam direction. Tracking detectors are expected to cover the entire z-range shown and the y-range between 25-75 cm approximately.

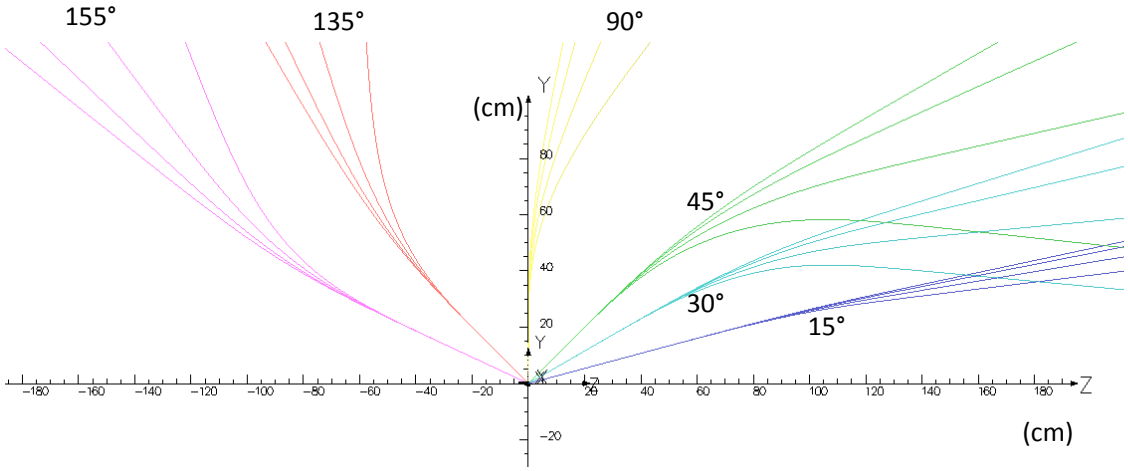

FIG. 11: Trajectories of elastic scattered electrons at 15^0, 30^0, 45^0, 90^0, 135^0, and 155^0. The four lines at a given angle correspond to the 1.035, 0.675, 0.450, and 0.338 MA-turns field configurations, respectively.

Fig. 12 shows the trajectories of 5, 10, and 30 MeV electrons emitted from the target center for the 0.675 MA-turns configuration. The angles range from 20^0 to 140^0 in steps of

40^0. The trajectories for the 1.035 (0.450) MA-turns are similar but they bend in about 5-6 cm before (after) the ones shown here. From Fig. 12 it appears that low-energy electrons (and positrons) from 25^0 to 165^0 can be detected within the tracking detector.

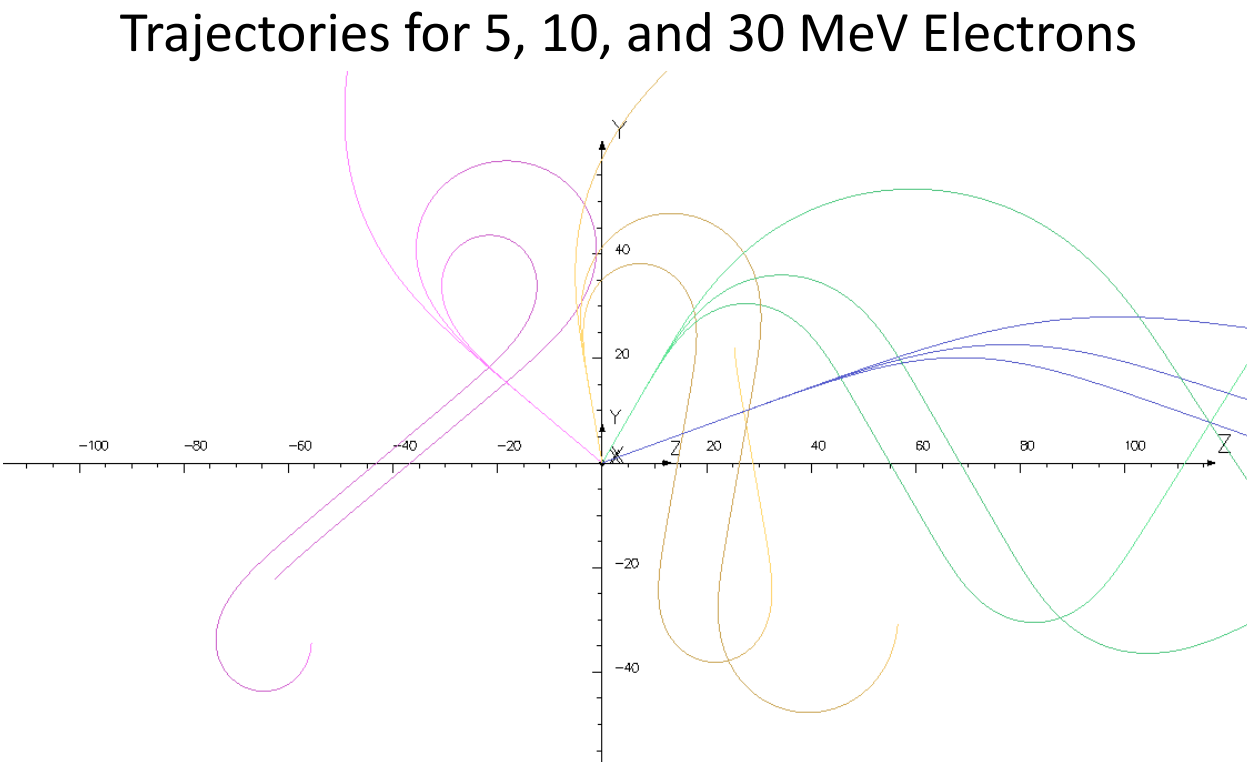

FIG. 12: Trajectories of 5, 10, and 30 MeV electrons emitted from the target center for the 0.675 MA-turns configuration. Dimensions are in cm and the trajectories are drawn in the yz plane. The angles range from 20^0 to 140^0 in steps of 40^0.

Below we present practical considerations for the 0.675 MA-turns configuration. We have chosen this configuration as a guidance because it represents at the moment a reasonable compromise between electron energy resolution and detection of low energy leptons.

The 0.675 MA-turns configuration requires 112.5 kA-turns/coil and a 1500 A/cm^2 current density for a total coil area of 75 cm^2; for typical 1 cm^2 conductors this implies a 1500 A operating current. To allow for water cooling the packing of copper conductors requires an area of about 1.3 times the conductor area. Since at room temperatures the copper density is limited to about 750 A/cm^2 this will require an area of about $2\times75\times1.3 = 195$ cm^2, i.e.,

Conductor in^2/cm^2	Turns/coil	Area Coil cm^2	R/coil Ω	Current A	V/coil Volts	Power kW
0.5^2/ 1.0	150 (6×25)	7.6×31.8	0.153	750	115	517.5
1.5^2/ 11.2	14 (2×7)	7.6×26.7	1.26×10^{-3}	8036	10.2	489.7

TABLE II: Operational parameters considering two types of available copper conductors for the 0.675 MA-turns configuration.

coils cross sections of approximately 6 cm by 35 cm.

Table II summarizes operational parameters for the 0.675 MA-turns configuration assuming two types of standard available conductors: a 0.5" by 0.5" copper with a conducting area of 1.0 cm^2 and a 1.5" by 1.5" copper with a conducting area of 11.2 cm^2. The latter were used for the BLAST spectrometer. For the first case it would require 150 turns per coil arrange in 6×25 configuration where in the second case 14 turns per coil are needed arranged in a 2×7 cross sectional configuration. The coil areas, operating currents and voltages shown in Table I give the range available for this configuration if normal temperature conductors were to be used. The consideration of liquid-nytrogen cooled copper conductors or superconducting wires would reduce the areas and power significantly although cooling powers would need to be provided.

C. Detectors

1. Drift chambers

For DarkLight, it is proposed to have in each of the six sectors drift chambers to measure the momenta, charges, scattering angles, and vertices for the leptons in the final state. This will be done by tracking the charged particles in three dimensions through the toroidal magnetic field and reconstructing the trajectories. Measuring the curvature of the tracks yields the particles' momenta, and the directions of curvature determine their charge. Tracing the particles' trajectories through the mapped magnetic field back to the target region allows the scattering angles, polar and azimuthal, to be determined. The position of closest approach to the beam axis is taken as the vertex position for the event. To maximize the active area, the drift chambers will be designed to fit between the coils of the toroidal magnet such

that the top and bottom plates of the drift chamber frame are in the shadow of the coils as viewed from the target. The drift chambers will have a large acceptance and nominally will subtend the polar angular range 25° to 165°. Thus, the chambers will be trapezoidal in shape.

The design of the DarkLight drift chambers will be guided by the design and experience with the BLAST drift chambers [54] shown in the photograph in Fig. 13. The BLAST drift chambers were designed at MIT, the large elements were constructed by industry, and the complete chambers were assembled, tested and commissioned at MIT. Each of the two horizontal sectors in the eight-coil BLAST contained three drift chambers (inner, middle, and outer) joined together by two interconnecting subsections to form a single gas volume. This was done so that only a single entrance and exit window was required for the combined drift chambers, thus minimizing energy loss and multiple scattering. Each of the three chambers consisted of top, bottom, and two end plates. Each plate was precisely machined from a solid aluminum plate and then pinned and bolted together to form each drift chamber. The positions of the feedthrough holes and twelve tooling balls set in inserts along the length of the top and bottom plates were measured with a coordinate measuring machine.

FIG. 13: One of the large acceptance drift chambers used in the BLAST experiment and now located at DESY for the upcoming OLYMPUS experiment.

2. Trigger scintillator

A scintillator hodoscope will be configured in each of the six sectors to trigger on the charged leptons. BLAST had such a system which provided a fast, stable timing signal correlated with the time of each event at the target independent of which scintillator was struck. This signal was used to trigger the readout and data acquisition system for all other components and particularly provided the COMMON STOP signal for the drift chambers. This permitted relative timings among all components to be measured. The TOF detector also provided a measure of energy deposition to aid particle identification. Approximate position information was also possible from the timing difference between the top and bottom photomultiplier tubes.

For this experiment, the trigger scintillator will predominantly trigger the scattered electrons. If an A' is produced, it is assumed to decay into an e^+e^- pair, and we have three leptons in the final state which sum to the 100 MeV beam energy, ignoring the kinetic energy of the proton. If the mass of the A' is low the scattered electron energy is close to the beam momentum. In all cases the sum of the energies of leptons reaching the trigger scintillator will be an appreciable fraction of the beam energy.

Bicron6 BC-408 plastic scintillator was chosen for its fast response time (0.9 ns rise time) and long attenuation length (210 cm). Each TOF scintillator bar was read out at both ends via Lucite light guides coupled to 3-inch diameter Electron Tubes7 model 9822B02 photomultiplier tubes equipped with Electron Tubes EBA-01 bases. The light guides were bent to point away from the interaction region so the PMTs would be roughly perpendicular to the toroidal magnetic field. Mu-metal shielding was used around all PMTs. The bases had actively stabilized voltage dividers so that the timing was independent of the gain.

The critical energy of plastic scintillator is 109 MeV, such that for the electron energies under consideration for a 100 MeV FEL experiment, the collision loss always dominates over the radiative losses.

3. Gas TPC

It is proposed to employ a gas TPC based on the BONUS technology developed at Jefferson Lab [57] to detect the low energy recoil protons in the final state. As seen in

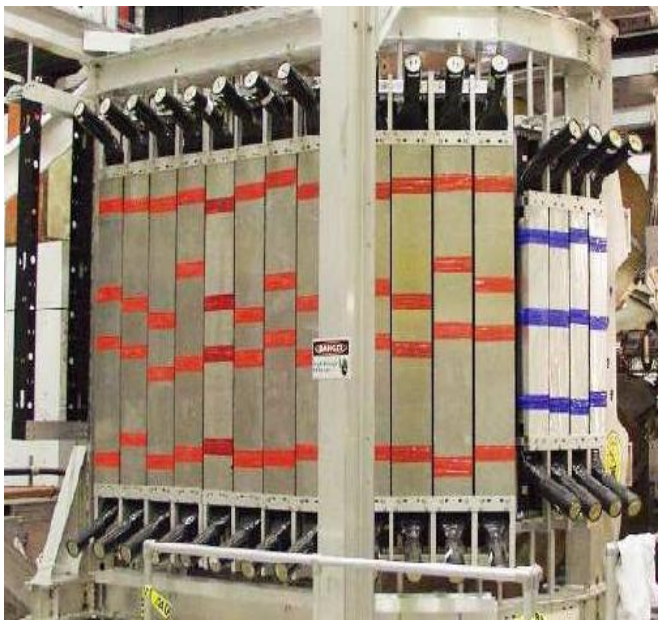

FIG. 14: The timing scintillators used in the BLAST experiment and now located at DESY for the upcoming OLYMPUS experiment.

Fig. 15, this detector has the capability to detect protons down to about 1 MeV. The gas target would be contained within the TPC, and is foreseen to be made of kapton with 30 μm or less target walls. For the eg6 experiment a kapton tube, 6 mm in diameter with 30 μm walls was used, where the target cell could be filled up to a pressure of 7.5 atm. In our case, we have a differential presure of at most 1 atm. Thus, we can design a target and gas TPC to efficiently detect protons down to 1 MeV kinetic energy.

The BONUS and followup BONUS/eg6 detector systems were cylindrically symmetric (see Fig. 16) around the beamline, and extended to a radius of 10 cm. Readout was in the radial direction. We have budgeted a similar 10 cm radius for the recoil proton detector, but hope to be able to do readout on the front and back sides of the cylinder rather than radially outward. This requires further study of the electronics artwork. Compared to the BONUS setup, our requirements are somewhat simplified. Due to the specific elastic scattering kinematics, both scattered electrons and recoiling protons will have predominant rates at large angles. Thus, we do not foresee the need to have small-angle coverage (below 15° or so), alleviating Moller contamination. Furthermore, The BONUS detector resided

in a large solenoidal magnetic field. This helped "bottle up" the Moller electrons, but also meant that tracking of the protons became cumbersome as one needs to deal with Lorentz angles. Thus, BONUS and eg6 employed a radial TPC. For the DarkLight experiment, we need to also measure relatively low-energy electrons and positrons (down to 5 MeV or so) following the A$'$ decay, and can not afford large magnetic fields. For the proposed toroid, the envisioned TPC would reside entirely in a fringe field region away from the magnet coils. Thus, we only need the cylindrical GEM detectors to act as a regular TPC, and will obtain our momentum resolution solely from dE/dx energy loss. For the BONUS experiment, the corresponding momentum resolution was 18% (σ). Given that our region of interest will be low-Q^2 elastic scattering (where the rates are largest) only, we envision to only have to detect recoil protons between 1 and 9 MeV (50 and 150 MeV/c momentum), and thus this momentum resolution is sufficient.

For the BONUS detector, the outermost cylindrical layer was the readout board made of a flexible polymide substrate. It carries gold-plated conductive pads on the inner surface with a pattern of 4.45 mm $\times$ 5 mm. The pads are connected by closed vias to the outer surface on which groups of 16 pads are traced to a common connector, carrying 16-channel preamplifier cards. Given the approximate 5 mm pad size and a radial distance of about 10 cm, this would result in an angular resolution of about 1.5°. This is indeed close to the empirical σ_ϕ of the BONUS experiment: 0.025 rad (σ). We may reduce the pad size and increase the number of readout channels to further improve this resolution.

A data acquisition of a radial TPC is in general limited by the drift speed. The BONUS experiment used a relatively slow gas mixture of 80% helium and 20% dimethyl ether (10 μ/ns), where fast gases typically have 50 μ/ns. The eg6 experiment (detecting recoiling helium nuclei) used 80% neon and 20% dimethyl ether to improve the energy loss dE/dx resolution inside the drift gas. We will also consider using hydrogen gas, which may be sufficient for our detection of low-energy recoil protons through dE/dx in a regular TPC, to alleviate any gas diffusion issues with the hydrogen gas target.

In the BONUS experiment, the radial TPC detector signals were inverted on the preamplifier cards and transmitted via 6 m long cables to a low-impedance receiver circuit, feeding the positiive signals into the readout electronics developed at CERN for the TPC of the ALICE experiment. The ALICE standard readout hardware features optical data links and controls. Each readout card provides 128 channels of pre-amplification, digitization via a

10-bit ADC, signal correction circuits, and a pipeline buffer for eight events. For the eg6 experiment, the readout was grouped into six branches, each controlled by one readout controller, with four readout cards per branch. This resulted in a data acquisition rate of 3 kHz. For the present experiment, we believe even higher rates, up to 10 kHz, should be possible, as we do not require a radial TPC. This is well matched to the expected trigger rate within the angular range of the experiment.

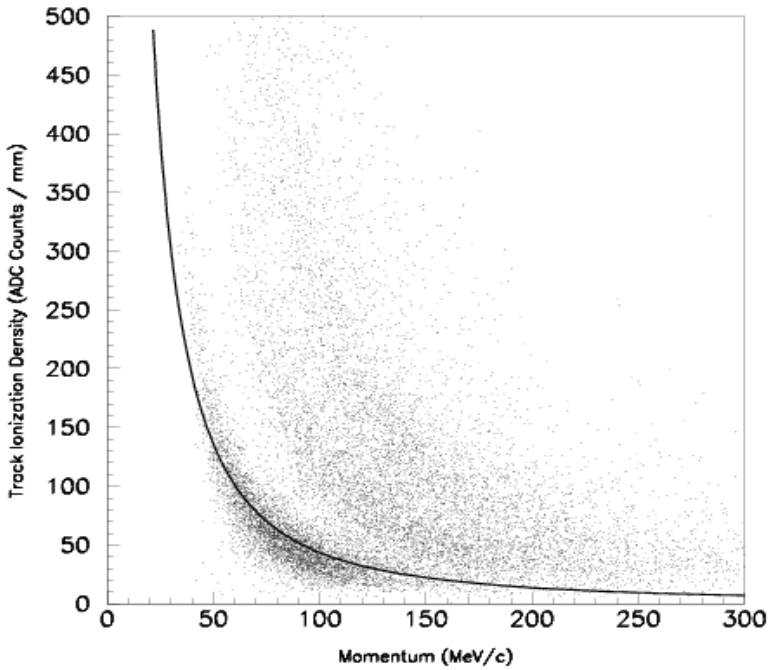

FIG. 15: Track ionization density vs. momentum [57]. The lowest band is consistent with the $\frac{dE}{dx}$ expected for protons. The curve is the prediction of the Bethe-Bloch formula for protons.

4. Inner vertex detector

Outside the gas TPC, there will be further layers of GEM detectors. These will provide a dual function: to detect the low-energy (5 MeV or so) electrons and positrons that will already curl up in the fringe fields of the proposed toroid, and to provide a vertex for the final-state leptons. GEMs have been developed at MIT[58] for the forward tracker upgrade of the STAR detector at RHIC. In addition, these are being constructed for the OLYMPUS experiment at DESY[55]. This inner vertex detector will provide a vertex measurement of the final-state leptons with a precision of $\pm 100\mu$ m. Unlike the GEM detectors in the gas

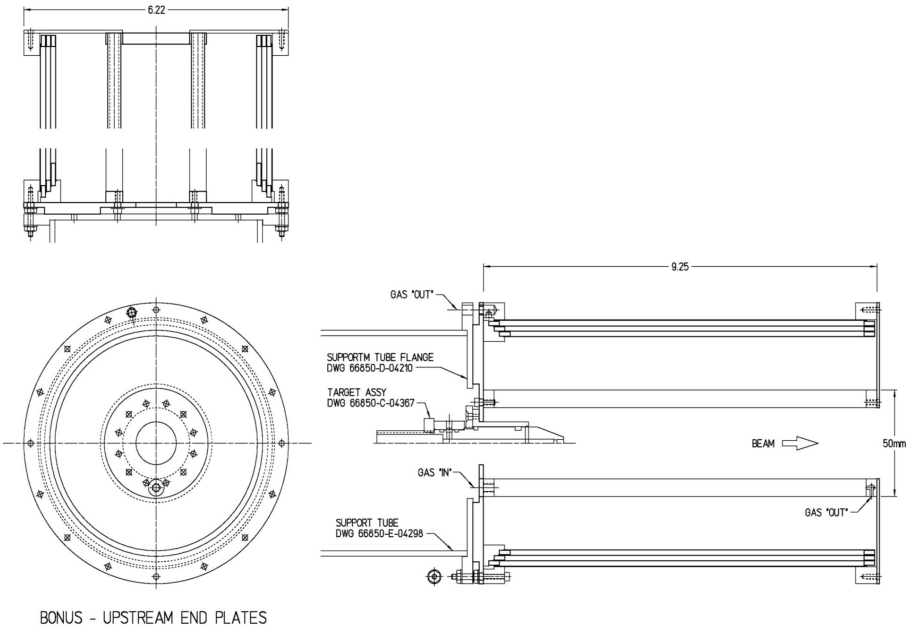

FIG. 16: Drawings of the BONUSII detector used in the eg6 run in October 2009. Compared to the earlier BONUS detector, the newly developed radial TPC for the eg6 experiment featured an improved mechanical support for the GEM foils and readout plane. Also, continuous foils were used for each GEM plane cylinder, removing blind spots and increasing the azimuthal acceptance of the detector.

TPC above, the voltages of these GEM detectors will be chosen such that they are sensitive to minimum-ionizing particles and the GEM detector's fine segmentation make them suitable for a high rate environment.

D. Internal target

1. Concept

To achieve the desired luminosity of 6×10^{35} cm^{-2} s^{-1} with the 10 mA Jefferson Laboratory FEL beam, a target of about 10^{19} hydrogen atoms cm^{-2} is required. We propose to generate the target thickness for DarkLight by flowing hydrogen gas through a cryogenically cooled, thin-walled vessel through which the FEL beam passes. Figure 17 shows the schematic layout of such a target. Hydrogen gas flows at a rate of F atoms/sec into a cell

and exits symmetrically along conductance tubes of length L and inner diameter D. The central density in equilibrium is ρ_0 atoms cm^{-3}. The FEL electron beam passes through the tubes and storage cell. There will be a need for differential pumping both upstream and downstream of the target. Note that the target thickness increases inversely as the fourth power of D, assuming a cylindrical tube.

With a flow rate of F $= 1.5 \times 10^{18}$ s^{-1} (0.1 torr-liter/sec) a tube of length L = 30 cm and D = 2 mm is required to produce $\rho_0 = 10^{18}$ cm^{-3}. Over a length of 10 cm this can produce a target of thickness 10^{19} cm^{-2}. The average target pressure in the storage cell is estimated as 100 torr.

A clear issue with this approach is the scattering of beam halo from the cell. The FEL beam profile has a central Gaussian core of width ≈150 microns but there will also be a non-Gaussian tail which can strike the incident conductance tube. There will be a need for collimation upstream of the storage cell. It will be important to design the beam optics here to minimize the beam size at the target location. Track reconstruction to identify the vertex in the storage cell will reject background events.

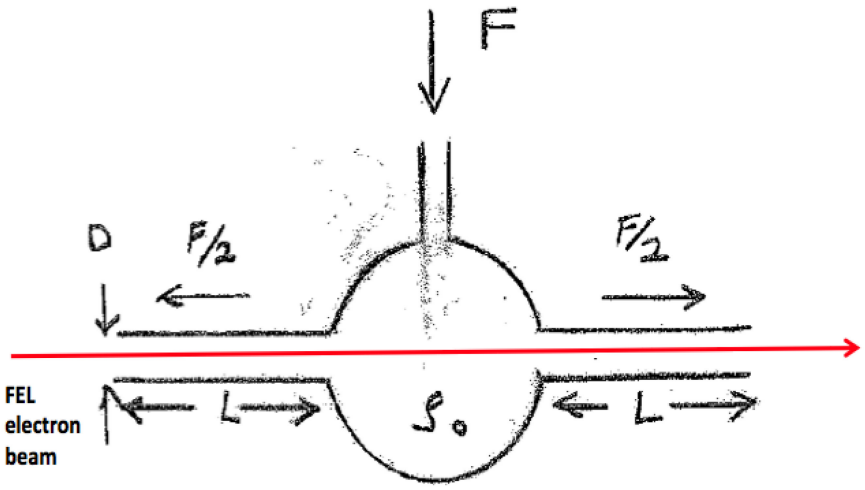

FIG. 17: Schematic layout of the storage cell target.

With the final-state ≈1 MeV protons having to exit the storage cell, the thickness of the target cell must be very thin. We assume 30 μm of kapton, as was used in the recent CLAS/eg6 run using an upgraded BONUS detector.

A three-stage differential pumping system on each side of the gas target is required to pump away the gas and interface to the $\approx 10^{-9}$ torr vacuum pressure of the FEL. This is

accomplished with magnetically levitated turbomolecular pumps which are located outside the strong magnetic field of the DarkLight toroid.

2. Beam interaction with the target

Calculations of the interaction of the 100 MeV electron beam and the gas target have been carried out for both hydrogen and xenon targets. While DarkLight is initially proposed using a hydrogen target, the possibility to use a heavier gas target is also considered. Two processes contribute significantly to energy loss, and two processes contribute significantly to electron loss due to beam spreading.

Ionization: The energy loss for an electron traveling through a material due to ionization is given by this version of the Bethe-Bloch equation [59]:

$$-\frac{dE}{dx} = 2\pi r_e^2 m_e c^2 \rho Z \frac{1}{\beta^2} l \left[\ln \frac{\tau^2(\tau+2)}{2(I/m_e c^2)^2} + F(\tau) - \delta - 2\frac{C}{Z} \right] \tag{4}$$

$$F(\tau) = 1 - \beta^2 + \frac{\frac{1}{8}\tau^2 - (2\tau+1)\ln 2}{(\tau+1)^2} \tag{5}$$

where τ is the kinetic energy of the electron in units of the electron mass.

The electrons are energetic enough that the shell-correction is definitely negligible ($C = 0$). The mean excitation potentials are $I_{\mathrm{H}} \approx 19$ eV and for Xenon is $I_{\mathrm{Xe}} \approx 482$ eV.

From [60], we can estimate the density effect in hydrogen with:

$$\delta_{\mathrm{H}} = 4.6X - 9.6 + 0.035(3.5 - X)^{6.79} \tag{6}$$

$$\delta_{\mathrm{Xe}} = 4.6X - 12.7 + 0.133(5.0 - X)^{3.02} \tag{7}$$

When $X = \log_{10}(\beta\gamma) = \log_{10}(200) \approx 2.30$, we get $\delta_{\mathrm{H}} \approx 1.2$ and $\delta_{\mathrm{Xe}} \approx 0.6$. Thus, we get that the energy loss due to ionization is

$$\Delta E_{\mathrm{H}}/\sigma_{\mathrm{H}} = (2.6 \times 10^{-25}\ \mathrm{MeV\ cm^2})34.5 \approx 8.8 \times 10^{-24}\ \mathrm{MeV\ cm^2} \tag{8}$$

$$\Delta E_{\mathrm{Xe}}/\sigma_{\mathrm{Xe}} = (1.4 \times 10^{-23}\ \mathrm{MeV\ cm^2})28.6 \approx 4 \times 10^{-22}\ \mathrm{MeV\ cm^2} \tag{9}$$

For a target of thickness 10^{19} hydrogen atoms cm^{-2}, these energy losses are negligible.

Bremsstrahlung: When $E_0 \gg 137 m_e c^2 Z^{-1/3}$, we can use complete screening as an approximation. The differential cross section is given by:

$$\frac{d\sigma}{d\omega} \approx 4\frac{\alpha r_0^2}{\omega} Z(Z+1)\left[\left(1-\frac{2}{3}\varepsilon+\varepsilon^2\right)\ln\frac{183}{Z^{1/3}}+\frac{1}{9}\varepsilon\right] \tag{10}$$

where $\varepsilon = (E_0 - \hbar\omega)/E_0$. The energy loss is given by multiplying the cross subsection by the photon energy and integrating over all possible photon energies (approximately ε from 0 to 1):

$$-\left(\frac{dE}{dx}\right) = N\int_0^{E_0/\hbar} \hbar\omega \frac{d\sigma}{d\omega} d\omega = NE_0\alpha r_0^2 Z(Z+1)\left(\frac{1}{18}+\ln 183\right) \tag{11}$$

Thus, the energy loss over the cross-sectional density is

$$\Delta E_{\mathrm{H}}/\sigma_{\mathrm{H}} \approx 4\times 10^{-25}\,\mathrm{MeV\ cm^2} \tag{12}$$

$$\Delta E_{\mathrm{Xe}}/\sigma_{\mathrm{Xe}} \approx 7\times 10^{-22}\,\mathrm{MeV\ cm^2} \tag{13}$$

Again, for the design target thickness of 10^{19} hydrogen atoms cm^{-2}, these energy losses are negligible.

Mott Scattering: Since the mass of the nucleus is large compared to the energy of the electron, we will neglect recoil of the proton and use the center-of-mass Mott cross subsection:

$$\frac{d\sigma}{d\Omega} = \left(\frac{Ze^2}{2E}\right)^2 \frac{\cos^2\theta/2}{\sin^4\theta/2} \tag{14}$$

Integrating over the solid angle:

$$\sigma = (6\times 10^{-30}\,\mathrm{cm^2})Z^2\int_{\theta_c}^{\pi}\cot^3(\theta/2)d\theta \approx (2\times 10^{-29}\,\mathrm{cm^2})Z^2{\theta_c}^{-2} \tag{15}$$

θ_c is the acceptance angle for the beam after interaction with the target. A conservative estimation of $\theta_c \approx 5\,\mathrm{mrad}$ gives the cross subsection for hydrogen as 8×10^{-25} cm^2 and for xenon as 2×10^{-21} cm^2.

Møller Scattering: The scattering angle of the higher-energy electron is given by:

$$\cos^2\theta = \frac{(E_0+mc^2)(E_0-E)}{(E_0-mc^2)(E_0-E+2mc^2)} \tag{16}$$

and for the lower-energy electron:

$$\cos^2\theta' = \frac{(E-mc^2)(E_0+mc^2)}{(E_0-mc^2)(E+mc^2)} \tag{17}$$

as determined by kinematics, where E is the final energy of the electron initially at rest. The total cross subsection is

$$\sigma = 2\pi \frac{Z^2 e^4}{mc^2} \int_{E_c - mc^2}^{E_0/2} \frac{1}{E^2} dE \tag{18}$$

to first order. $\theta_c \approx 5\,\text{mrad}$ corresponds to an energy of $E_c - mc^2 \approx 0.25$ MeV. Thus, the total cross section for hydrogen is 2×10^{-25} cm^2 and for xenon is 5×10^{-22} cm^2.

At the design target thickness, the total fractional beam loss due to scattering is a thousandth of a percent for hydrogen and several percent for xenon.

E. Detector Integration

The pit on the UV line where the Cornell wiggler is now located appears to be a suitable location for the DarkLight experiment. Fig. 18 shows a schematic layout of the experiment in this location. In this layout, we have not added the foreseen tracking chambers or trigger scintillators yet. The toroid conveniently fits in the existing pit. Differential pumping ports can also easily be accomodated in the vacuum system, as shown in Fig. 19. We would likely need a mezzanine platform for servicing of the two pumps closest to the interaction region, similar as in the BLAST experiment. The four outermost pumping stations (two on each side) may be changed to go downwards rather than upwards, if space permits.

Fig. 20 shows a schematic layout of the target and inner tracker region for DarkLight. The gas TPC is connected directly to the gas target to minimize any amount of material the recoil protons meet on their way into the BONUS-type detector. We have budgeted a 10 cm (radius) cylindrical region for this recoil proton detector. A second cylinder of detectors aims to map the low-energy (down to 5 MeV) electrons and positrons before they enter the high-field region of the toroid magnet. Even in the fringe field of the toroid, fields can become appreciable for such low-momentum particles. This region will also have GEM-type tracking chambers, but with voltages to allow detection of minimum-ionizing particles.

F. Trigger

The resonance signal of A' decay lies on top of a large QED background and both lie on top of an even larger elastic scattering and Møller rate. These large rates require a trigger

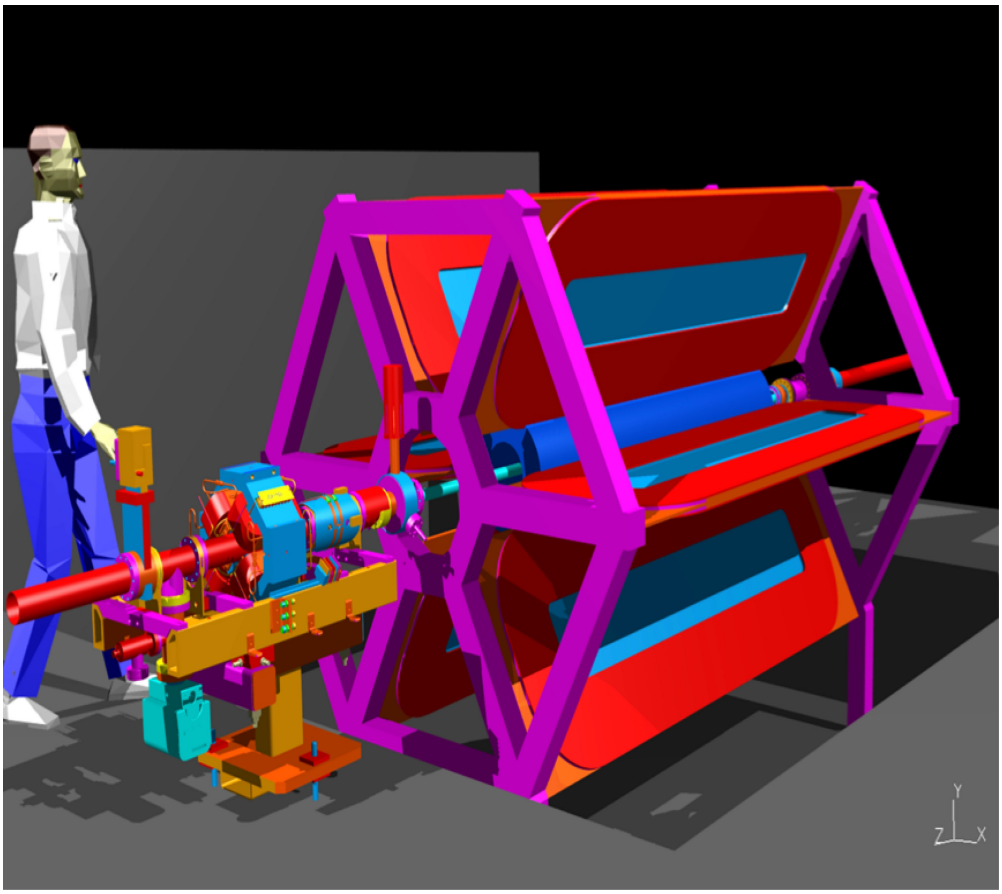

FIG. 18: Schematic layout of the DarkLight experiment.

able to select events with a proton and three leptons in the final state. We have developed a trigger scheme and detector geometry that excludes the highest rates of elastic and Møller scattering at low angles while keeping the data rate to disk at around 10 kHz. The DarkLight trigger concept is as follows:

- The tracker is instrumented from $25° < \theta_\ell < 165°$, excluding most of the high rate elastic and M øller scatters. The TPC for detecting protons covers from $5° < \theta_p < 89°$, avoiding the large rate of protons at 90∘ from elastic scattering. Because of the toroid coils, there is a modest 13% loss of azimuthal coverage per electron/positron track. To be considered for triggering, a lepton must reach the scintillator hodoscope, and therefore must have momentum greater that around 5 MeV.

- Requiring one "backwards" lepton with $\theta_\ell > 50∘$ reduces the total rate to around 10 MHz. This cut could be made using the scintillator hodoscope on the outside of the tracker which will give good timing resolution.

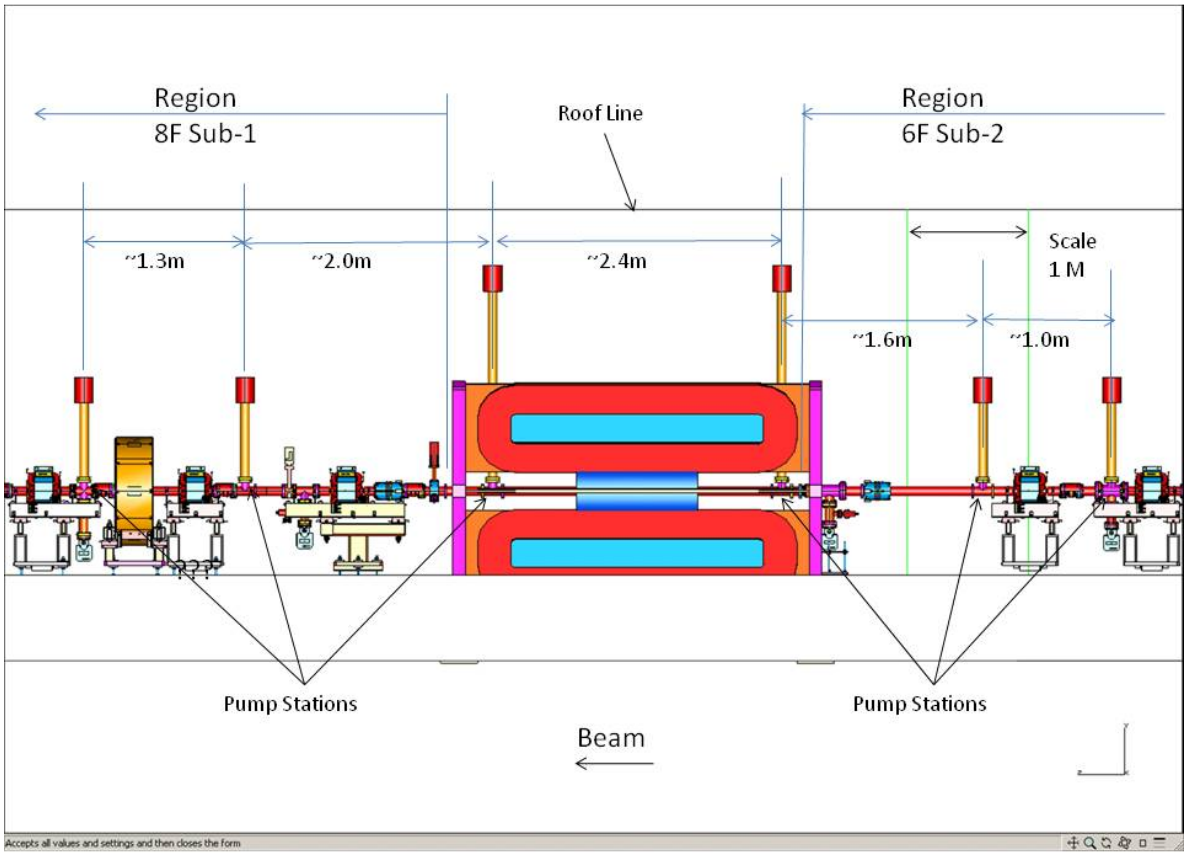

FIG. 19: Schematic layout of the differential pumping system of the DarkLight experiment sandwiching the UV line pit.

- Requiring at least two leptons in addition to the "backwards" lepton in a 10 nanosecond timing window further reduces the total rate to 1.2 MHz. This requirement could also be imposed using hits from the scintillator hodoscope. This requirement would reduce the pileup background considerable.

- A final requirement of one of the tracks being a positively charged gives a total rate of 0.9 kHz. Imposing this requirement requires use of the tracker data and a fast fitting algorithm. In addition, we require an identified proton with momentum above 1 MeV.

Events satisfying these requirements will be written to disk, along with prescaled events excluding some of the requirements. For the tracker of the size we contemplate, an on-disk rate of 10 kHz should be possible, leaving flexibility in the trigger conditions given above.

The signal is a positron and electron with an invariant mass of $m_{e^+e^-} - m_{A'} < \delta m_{e^+e^-}$. Here $\delta m_{e^+e^-}$ is invariant mass resolution of e^+e^- pairs measured by tracker, taken conser-

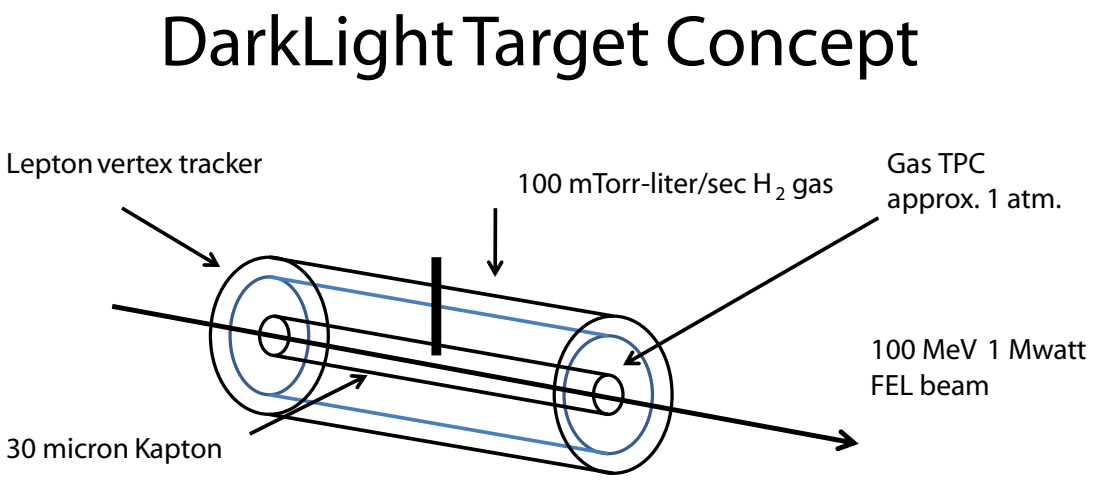

FIG. 20: Schematic layout of the DarkLight target and inner trackers.

vatively to be 500 keV which is achievable with the tracker and magnetic fields we have described above (see V). Assuming that dominant background is QED $ep \rightarrow ep\,e^+e^-$ we calculate where $S/\sqrt{B} > 5$ for a given $m_{A'}$. The coupling constant α' reach as a function of $m_{A'}$ is shown in Fig. 21. We are also investigating a trigger scheme for $ep \rightarrow ep +$ invisible.

V. EXPECTED PERFORMANCE

Reconstruction of all final state particles presents the major advantage and key challenge to the DarkLight experiment. The reconstruction of all final state particles will allow strong application of kinematic constraints, leading to high background rejection. A tracking system extending from 25 cm to 50 cm in cylindrical radius ρ and in the forward directions acts to identify the final state leptons and measure their momenta precisely.

The tracking study used an azimuthally symmetric toroidal field based on the six coil configuration shown in Fig. 10. A' events were simulated using initial state four vectors from [56]. Both leptons were required to have a polar angle larger than 25 degrees. The leptons from the A' decay were swum through the detector geometry by Simpson's rule integration of the Lorentz equation. Fig. 23 shows representative tracks. Hits were recorded at 1 cm ρ layers in the range 25 cm $< \rho <$ 50 cm for $|z|$ <25 cm and 10 cm $< \rho <$ 50 cm for 25 cm $< |z| <$50 cm. A Gaussian spatial variation with width 250 μm was applied to each hit.

Fig. 22 shows how the e^+e^- from the A' decay shares energy. Near the upper kinematic

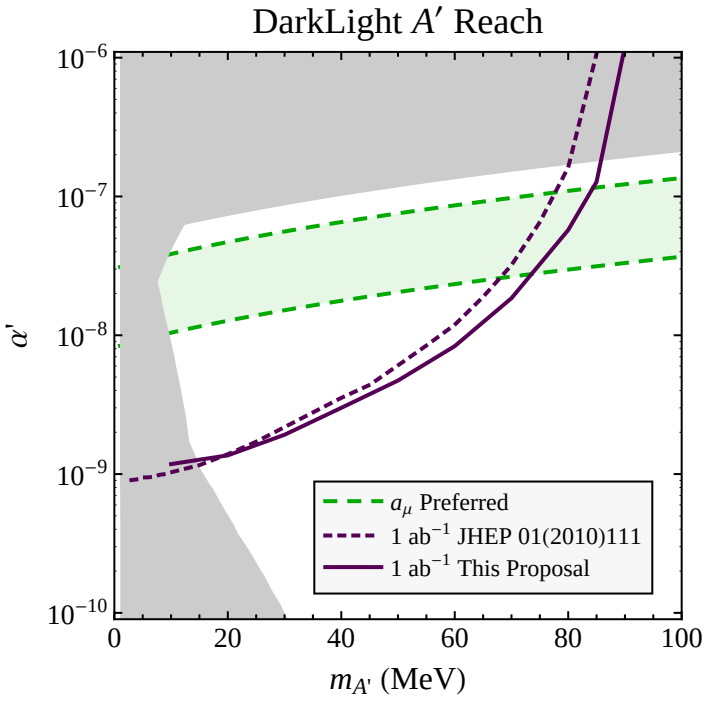

FIG. 21: α' sensitivity as a function of $m_{A'}$ assuming $\sigma_{e^+e^-} = 500$ keV, and the proposed triggering scheme and an integrated luminosity of 1/ab. The reach expected from a preliminary study in Ref. [56] is shown for comparison, with the improved reach at high $m_{A'}$ due to the larger forward proton acceptance from the gas TPC.

boundary of the A' mass of 92 MeV, the A' is nearly at rest and the leptons come out with similar energies around 40 MeV, while a the lower end of the kinematic range, the energies of the leptons may be very different. Since we determine the lepton energy by sampling the trajectory of the particle in a magnetic field, the resolution worsens for higher boson energies. Inspecting the trajectories in Fig. 23 shows that at higher fields, the lower energy leptons will not reach the trigger scintillators on the outside of the tracker, leading to lower efficiency for detecting those events. The first point argues for a larger bending power while that latter argues for lower bending power. With this in mind, we have carried out this study for bending powers of 0.05, 0.16 and 0.32 T-m as we may wish to run the experiment at different field settings to optimize different A' masses.

Material of thickness $x = 0.01X_o$ simulated multiple scattering at ρ=5 cm: at this point,

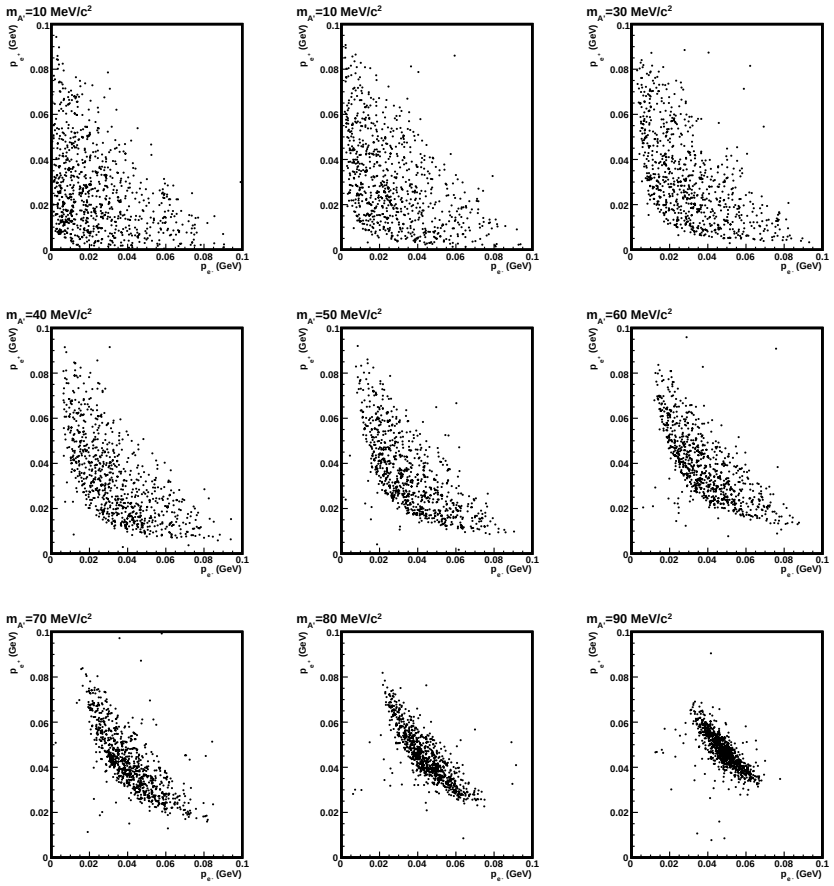

FIG. 22: Sharing of lepton momenta. Each scatter plot shows the reconstructed momenta of the e^+e^- pair from different A' masses..

a scattering angle was sampled from a Gaussian distribution with width

$$\theta = \frac{13.7MeV}{p\beta}\sqrt{x/X_o}.$$

The scattered momentum had the same magnitude as the momentum before scattering.

A five parameter $(x_o, y_o, p_x, p_y, p_z)$ swim was carried out on each of the two tracks using initial parameter values varied by 5% from the true parameter values. A first fit determined the momentum coordinated with the spatial coordinated fixed at the origin. A second fit with all five parameters free gave the fit values. The fit values determined the fit mass for the A'.

Figs. 24 and 25 show the momentum resolutions from the fit tracks over the kinematic range of the experiment. The momentum resolution ranges from 200 to 370 keV over the kinematic range.

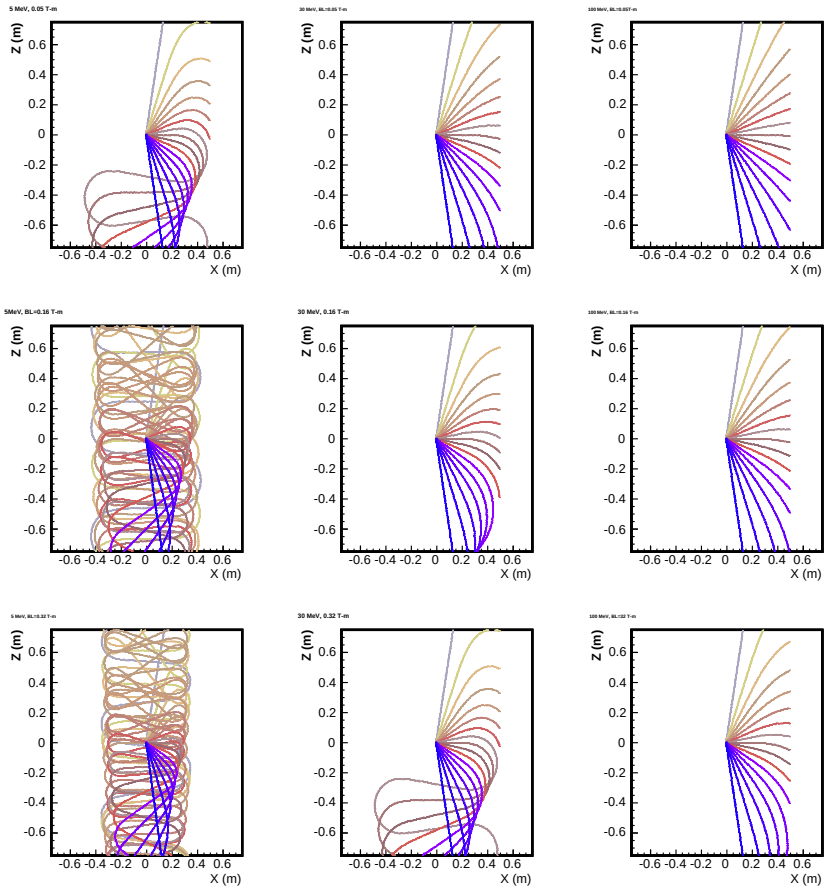

FIG. 23: Left column: lepton energy of 5 MeV. Middle: lepton energy of 3 MeV. Right: lepton energy of 100 MeV. Top row: bending pwoer of 0.05 T-m. Center row: BL=0.16 T-m. Bottom row: 0.32 T-m. In all panels, there are sixteen tracks with initial polar angles in 10 to 170 degrees in 10 degree steps.

Fig. 26 shows the fit masses for A' masses from 10-90 MeV with a bending power of 0.16 T-m. The typical resolution is 400-1300 keV. Varying the radial sampling frequency from 0.5 to 20 cm, and varying the spatial resolution in the range 100 to 500 μ has little effect on the width.

Fig. 27 shows the vertex resolution in a field with a bending power of 0.16 T-m. Typical values are 1–2 mm, with large non-Gaussian tails. The target volume is about 1 mm across, so the vertex resolution will need to be improved to allow determination of whether a given track starts from the target cell or not.

Fig. 28 shows the mass resolution for different bending powers. In the worse case, the tracker gives a mass resolution about a factor of two worse than our target of 1 MeV, leading

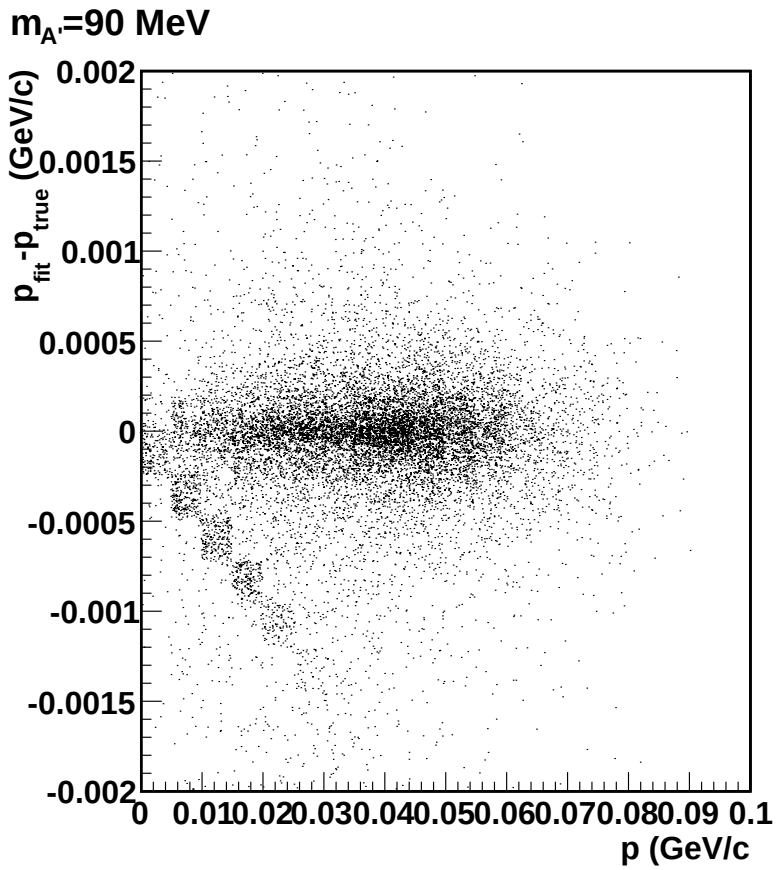

FIG. 24: Scatter plot of input momentum versus the difference between fit and input momentum for 0.16 T-m bending power. The squares of points going down from left to right result from reconstruction ambiguities in the forward region and constitute only a small part of the sample.

to a loss of sensitivity for higher A' masses. However, taking data at 0.05 T-m and 0.16 T-m would give good performance over the entire A' mass range.

This study shows that for realistic conditions, tracking in the range of 25 to 50 cm from the target cell will give sufficient mass resolution to meet the goals of the DarkLight experiment using 20 spatial samples with 200 μm spatial resolution, comparable to the performance of the BLAST wire chambers described above. The vertex resolution will need improvement to ensure the tracks originate from the target. Whether or not vertexing at this level is needed requires further study. The GEANT4 program used for this study will be extended to understand pattern recognition, pileup and the inner detector systems.

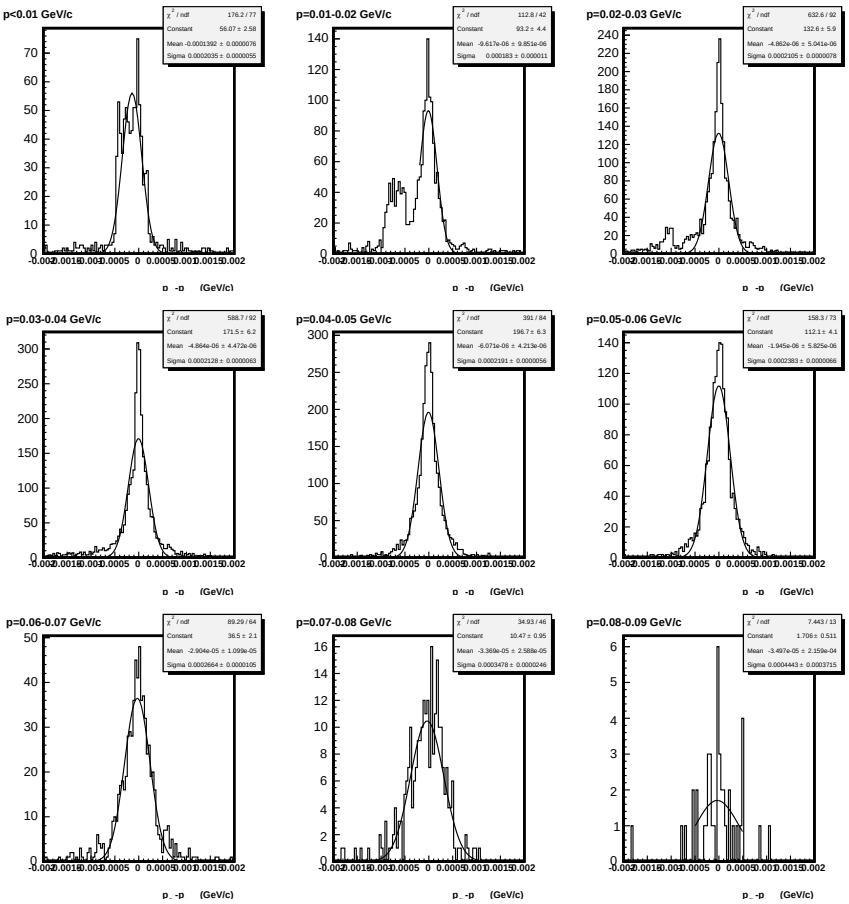

FIG. 25: Fit momentum residuals for 10 MeV momentum bins.

VI. REALIZATION

In this section, the major milestones on the path to realizing the experiment are identified.

A. Design of the Experiment

The concept described in this document for the DarkLight experiment must be developed into a complete technical design. This would allow a detailed and accurate costing of the necessary experimental equipment to be carried out. Once this is in hand, it is expected that this technical design would be reviewed in detail.

To complete the technical design of DarkLight will require appropriate engineering support as well as the participation of the physicists in the collaboration.

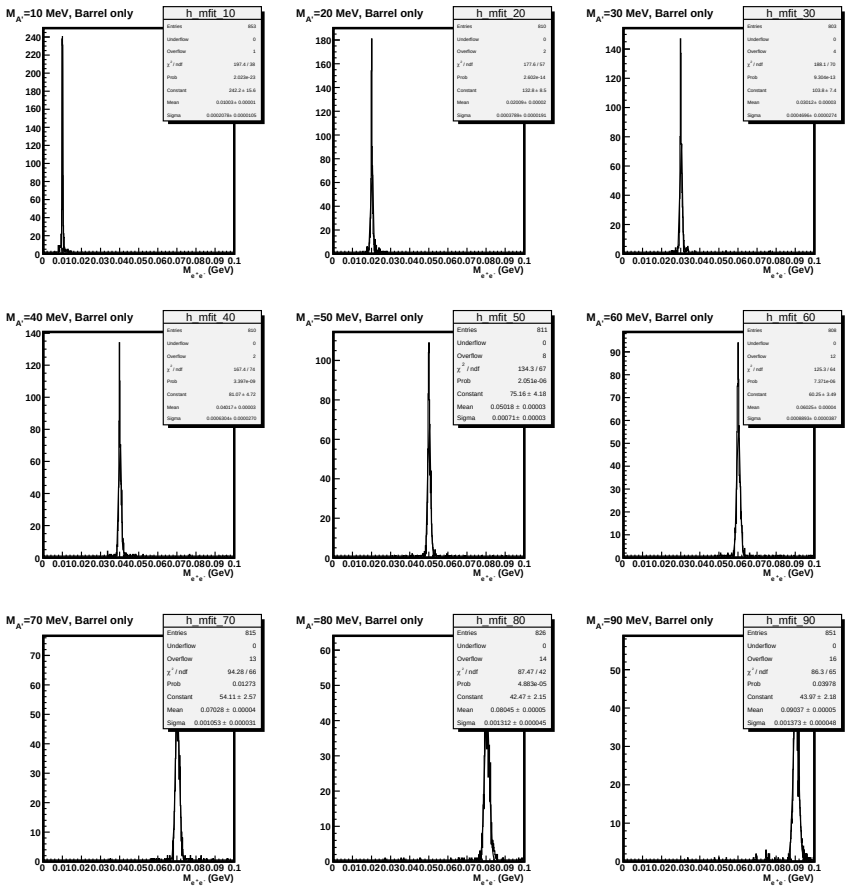

FIG. 26: Fit mass distributions for $m_{A'}$ =10–90 MeV.

B. Development of the required FEL Beam

An essential element in the path to realization of DarkLight is the development of the required 100 MeV FEL beam. It is anticipated that this will include optics development, halo and background studies, emittance measurements, and dedicated test runs to produce the intense, focused, low-halo beam required to pass through the target.

C. Resources

Resources will be required as follows:

- to support engineering of the experiment

  Assuming the science is endorsed at PAC37, the collaboration would like to proceed with the technical design of the experiment in a timely way. The cost of DarkLight is

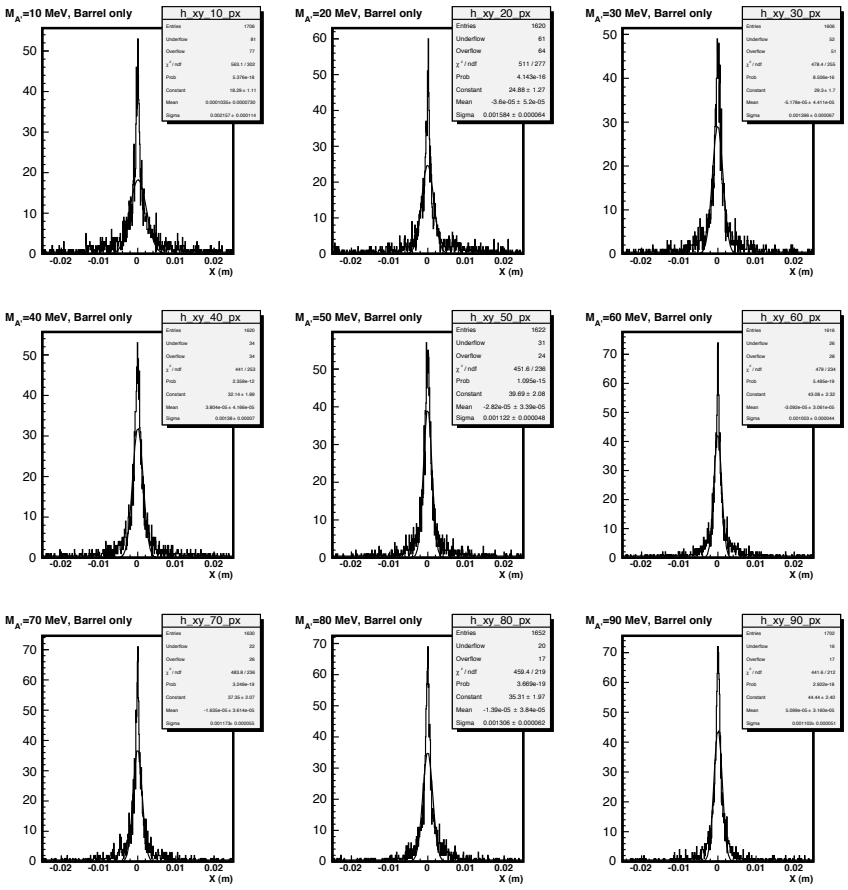

FIG. 27: x coordinate resolution from fit for $m_{A'}$ =10-90 MeV. The y distribution is identical.

judged to be in excess of $ 2 million and the construction project will need to follow the DOE order 413.3 A. It is estimated, based on previous experience with the BLAST and OLYMPUS experiments, that about 12 man-months of engineering (mechanical, electrical, and vacuum) and about 12 man-months of drafting will be required to bring DarkLight from CD-0, through CD-1 to CD-2.

- to develop the required FEL 100 MeV electron beam

  To make progress on the beam development, resources will be required to support FEL personnel and to provide for delivery of the FEL beam. We believe we will need the equivalent of 30 days running assuming 100% efficiency [62]

- An integrated luminosity of 1/ab at two different magnetic field settings. In terms of FEL running time, this translates to 60 days at 100% efficiency.

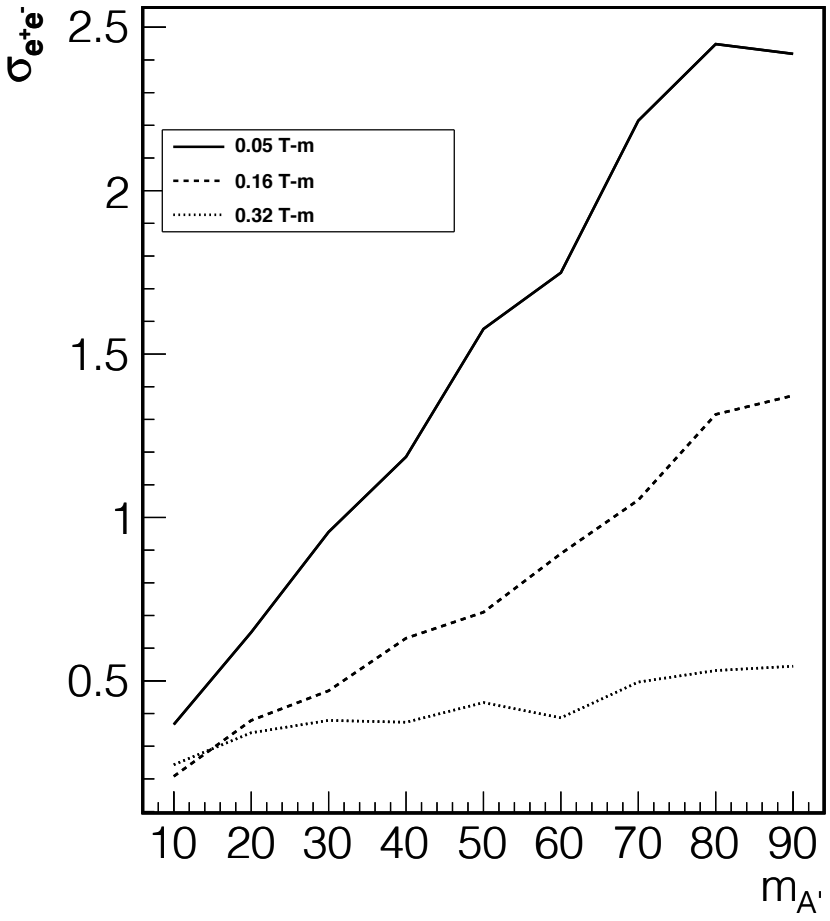

FIG. 28: Experimental mass resolution for bending powers of 0.05 T-m, 0.16 T-m and 0.32 T-m as a function of A' mass.

In addition, a sponsor for the running costs for the FEL, which at this time are provided by the Office of Naval Research, must be identified. The experiment will require time for beam development and tests as well as three months of dedicated data taking.

D. Schedule

A possible schedule to a full proposal is as follows:

- Science case endorsed January 2011
- Beam development begins March 2011
- Resources for technical design become available Fall 2011

- Technical review Summer 2012
- DarkLight construction begins Fall 2012
- DarkLight data taking begins 2015

VII. SUMMARY

The DarkLight experiment provides a unique opportunity to search for the A' boson that could explain the origin of dark matter. DarkLight will be a challenging experiment, but an achievable one in the coming five years. Over the same time, results from cosmic ray and nuclear recoil experiments and the LHC may shape a new picture of dark matter, one in which DarkLight will play a key role.

This proposal has laid out a scientific case for DarkLight and shown the experiment is technically feasible at the Jefferson Lab Free Electron Laser. We are asking for an endorsement for DarkLight from PAC37 in order to move forward with the design of the experiment in the coming years. An endorsement of DarkLight will also enable us to begin discussions with Jefferson Lab and the agencies for support of the project.

Our formal beam-time request at the FEL request to carry out the measurement we have proposed is for the equivalent of 60 running days (assuming 100% efficiency) for data taking and the equivalent of 30 running days (assuming 100% efficiency) for beam studies, check-out and calibration.

[1] V. C. Rubin and W. K. Ford, Jr., Astrophys. J. **159**, 379 (1970).

[2] J. K. Adelman-McCarthy et al. (SDSS), Astrophys. J. Suppl. **162**, 38 (2006), astro-ph/0507711.

[3] E. Komatsu et al. (WMAP), Astrophys. J. Suppl. **180**, 330 (2009), 0803.0547.

[4] U. G. Briel and J. P. Henry (1997), astro-ph/9711237.

[5] D. P. Finkbeiner and N. Weiner, Phys. Rev. **D76**, 083519 (2007), astro-ph/0702587.

[6] M. Pospelov, A. Ritz, and M. B. Voloshin, Phys. Lett. **B662**, 53 (2008), 0711.4866.

[7] N. Arkani-Hamed, D. P. Finkbeiner, T. R. Slatyer, and N. Weiner, Phys. Rev. **D79**, 015014 (2009), 0810.0713.

[8] Y. Nomura and J. Thaler (2008), 0810.5397.

[9] D. P. Finkbeiner (2004), astro-ph/0409027.

[10] D. Hooper, D. P. Finkbeiner, and G. Dobler, Phys. Rev. **D76**, 083012 (2007), 0705.3655.

[11] O. Adriani et al. (PAMELA), Nature **458**, 607 (2009), 0810.4995.

[12] A. A. Abdo et al. (The Fermi LAT), Phys. Rev. Lett. **102**, 181101 (2009), 0905.0025.

[13] F. Aharonian et al. (H.E.S.S.), Phys. Rev. Lett. **101**, 261104 (2008), 0811.3894.

[14] F. Aharonian et al. (H.E.S.S.) (2009), 0905.0105.

[15] G. Weidenspointner et al., Astron. Astrophys. **450**, 1013 (2006), astro-ph/0601673.

[16] J. Knodlseder et al., Astron. Astrophys. **411**, L457 (2003), astro-ph/0309442.

[17] R. Bernabei et al. (DAMA), Eur. Phys. J. **C56**, 333 (2008), 0804.2741.

[18] P. Meade, M. Papucci, and T. Volansky (2009), 0901.2925.

[19] J. Mardon, Y. Nomura, and J. Thaler, Phys. Rev. **D80**, 035013 (2009), 0905.3749.

[20] P. Meade, M. Papucci, A. Strumia, and T. Volansky (2009), 0905.0480.

[21] M. Davier, A. Hoecker, B. Malaescu, and Z. Zhang, ArXiv e-prints (2010), 1010.4180.

[22] N. Borodatchenkova, D. Choudhury, and M. Drees, Phys. Rev. Lett. **96**, 141802 (2006), hep-ph/0510147.

[23] P. Fayet, Phys. Rev. **D75**, 115017 (2007), hep-ph/0702176.

[24] B. Batell, M. Pospelov, and A. Ritz (2009), 0903.0363.

[25] R. Essig, P. Schuster, and N. Toro (2009), 0903.3941.

[26] M. Reece and L.-T. Wang (2009), 0904.1743.

[27] D. E. Morrissey, D. Poland, and K. M. Zurek (2009), 0904.2567.

[28] P.-f. Yin, J. Liu, and S.-h. Zhu (2009), 0904.4644.

[29] E. M. Riordan et al., Phys. Rev. Lett. **59**, 755 (1987).

[30] A. Bross et al., Phys. Rev. Lett. **67**, 2942 (1991).

[31] J. D. Bjorken, R. Essig, P. Schuster, and N. Toro (2009), 0906.0580.

[32] R. Essig, P. Schuster, N. Toro, and B. Wojtsekhowski (2010), 1001.2557.

[33] Y. Kahn, M. Schmitt, and T. M. P. Tait, Phys. Rev. **D78**, 115002 (2008), 0712.0007.

[34] M. Pospelov (2008), 0811.1030.

[35] E. Abouzaid et al. (KTeV), Phys. Rev. **D75**, 012004 (2007), hep-ex/0610072.

[36] B. Wojtsekhowski, AIP Conf. Proc. **1160**, 149 (2009), 0906.5265.

[37] C. Boehm and P. Fayet, Nucl. Phys. **B683**, 219 (2004), hep-ph/0305261.

[38] C. Boehm, D. Hooper, J. Silk, M. Casse, and J. Paul, Phys. Rev. Lett. **92**, 101301 (2004), astro-ph/0309686.

[39] C. Boehm, P. Fayet, and J. Silk, Phys. Rev. **D69**, 101302 (2004), hep-ph/0311143.

[40] P. Fayet, Phys. Rev. **D70**, 023514 (2004), hep-ph/0403226.

[41] S. Heinemeyer, Y. Kahn, M. Schmitt, and M. Velasco (2007), 0705.4056.

[42] R. Pohl et al., Nature **466**, 213 (2010).

[43] I. Sick, Phys. Lett. **B576**, 62 (2003), nucl-ex/0310008.

[44] P. G. Blunden and I. Sick, Phys. Rev. **C72**, 057601 (2005), nucl-th/0508037.

[45] J. C. Bernauer, P. Achenbach, C. Ayerbe Gayoso, R. Böhm, D. Bosnar, L. Debenjak, M. O. Distler, L. Doria, A. Esser, H. Fonvieille, et al., ArXiv e-prints (2010), 1007.5076.

[46] K. Melnikov and T. van Ritbergen, Physical Review Letters **84**, 1673 (2000), arXiv:hep-ph/9911277.

[47] T. Udem et al., Phys. Rev. Lett. **79**, 2646 (1997).

[48] P. J. Mohr, B. N. Taylor, and D. B. Newell, Reviews of Modern Physics **80**, 633 (2008), 0801.0028.

[49] G. R. Neil et al., Phys. Rev. Lett. **84**, 662 (2000).

[50] C. Tennant, in *TH3PBI03, Proceedings of PAC09* (2009).

[51] H. Zhang et al., in *WECNB03, BIW2010, Santa Fe, NM* (2010).

[52] D. Douglas, Tech. Rep., Jefferson Lab (2010).

[53] S. Zhang, in *Energy-recovery-linac Workshop, Ithaca, New York* (2009).

[54] D. Hasell et al., Nucl. Instrum. Meth. **A603**, 247 (2009).

[55] URL `http://web.mit.edu/olympus/`.

[56] M. Freytsis, G. Ovanesyan, and J. Thaler, JHEP **01**, 111 (2010), 0909.2862.

[57] H. C. Fenker et al., Nucl. Instrum. Meth. **A592**, 273 (2008).

[58] F. Simon et al., Nucl. Instrum. Meth. **A598**, 432 (2009).

[59] W. Leo, *Techniques for Nuclear and Particle Physics Experiments* (Springer, 1987).

[60] R. M. Sternheimer, S. M. Seltzer, and M. J. Berger, Phys. Rev. B **26**, 6067 (1982).

[61] In this context, the A' is often referred to as a U-boson.

[62] This number assuming 100% efficiency for both the detector and FEL. The number of calendar days in our request will depend on operational considerations for the FEL.